

MECHANICAL PROPERTIES OF Ti6Al4V PARTS PRODUCED BY  
ELECTRON BEAM MELTING AND TOPOLOGY OPTIMIZATION IN  
DIFFERENT BUILDING DIRECTIONS

A THESIS SUBMITTED TO  
THE GRADUATE SCHOOL OF NATURAL AND APPLIED SCIENCES  
OF  
MIDDLE EAST TECHNICAL UNIVERSITY

BY

SELEN TEMEL YİĞİTBAŞI

IN PARTIAL FULFILLMENT OF THE REQUIREMENTS  
FOR  
THE DEGREE OF MASTER OF SCIENCE  
IN  
MECHANICAL ENGINEERING

NOVEMBER 2018



Approval of the thesis:

**MECHANICAL PROPERTIES OF TI6AL4V PARTS PRODUCED BY  
ELECTRON BEAM MELTING AND TOPOLOGY OPTIMIZATION IN  
DIFFERENT BUILDING DIRECTIONS**

submitted by **SELEN TEMEL YİĞİTBAŞI** in partial fulfillment of the requirements  
for the degree of **Master of Science in Mechanical Engineering Department, Middle East Technical University** by,

Prof. Dr. Halil Kalıpçılar  
Dean, Graduate School of **Natural and Applied Sciences**

\_\_\_\_\_

Prof. Dr. M.A.Sahir Arıkan  
Head of Department, **Mechanical Engineering**

\_\_\_\_\_

Assoc. Prof. Dr. E. İlhan Konukseven  
Supervisor, **Mechanical Engineering Department, METU**

\_\_\_\_\_

Dr. Orhan Gülcan  
Co-supervisor, **Structural Design, TAI**

\_\_\_\_\_

**Examining Committee Members:**

Assist. Prof. Dr. Kıvanç Azgın  
Mechanical Engineering Department, METU

\_\_\_\_\_

Assoc. Prof. Dr. Erhan İlhan Konukseven  
Mechanical Engineering Department, METU

\_\_\_\_\_

Prof. Dr. Oğuzhan Yılmaz  
Mechanical Engineering Department, Gazi University

\_\_\_\_\_

Assist. Prof. Dr. Ulaş Yaman  
Mechanical Engineering Department, METU

\_\_\_\_\_

Assist. Prof. Dr. Sezer Özerinç  
Mechanical Engineering Department, METU

\_\_\_\_\_

**Date:** 09.11.2018

**I hereby declare that all information in this document has been obtained and presented in accordance with academic rules and ethical conduct. I also declare that, as required by these rules and conduct, I have fully cited and referenced all material and results that are not original to this work.**

Name, Last Name: Selen Temel Yiğitbaşı

Signature :

## **ABSTRACT**

### **MECHANICAL PROPERTIES OF Ti6Al4V PARTS PRODUCED BY ELECTRON BEAM MELTING AND TOPOLOGY OPTIMIZATION IN DIFFERENT BUILDING DIRECTIONS**

Temel Yiğitbaşı, Selen

M.S., Department of Mechanical Engineering

Supervisor : Assoc. Prof. Dr. E. İlhan Konukseven

Co-Supervisor : Dr. Orhan Gülcan

November 2018, 84 pages

Titanium and its alloys are used in various industries due to their mechanical properties such as high corrosion resistance, high strength and low-density. However, utilization of parts made of titanium are limited since the lead time for raw material is long, they are hard to machine, and the machining costs are high. On the other hand, it is possible to produce complex parts with powder material by additive manufacturing techniques, and there is a growing interest in research on these new technologies. Electron Beam Melting, one of the additive manufacturing methods, gives chance to designers to develop complex parts that have comparable mechanical properties to the parts produced by conventional methods.

In the first part of this study, nine samples according to ASTM E8 standard were produced in different building directions (according to machine coordinate system X, Y and Z). To see surface imperfections effect on mechanical properties, one of the samples built in each direction were machined by lathe. After that, tensile test was performed, surface roughness was measured for each specimen and the fracture

surfaces were examined. As a result, it was observed that the parts built in vertical direction have better tensile properties.

In the second part of the thesis, to show that it is possible to produce light weight complex parts that satisfy the system function by additive manufacturing, topology optimization of an aircraft fitting was done with data from the experimental part. Two optimizations were performed for the parts to be manufactured in vertical and horizontal building directions. Location of the parts were determined according to the load cases and corresponding stress values. After optimization, newer designs with around 40% less weight were obtained without sacrificing the system performance requirement.

**Keywords:** Additive Manufacturing, Electron Beam Melting, building direction, tensile properties, Ti6Al4V, topology optimization, part orientation

## ÖZ

### **ELEKTRON IŞINI ERGİTME YÖNTEMİ İLE ÜRETİLEN Ti6Al4V PARÇALARIN FARKLI KURULUM YÖNLERİNDEKİ MEKANİK ÖZELLİKLERİ VE TOPOLOJİ OPTİMİZASYONU**

Temel Yiğitbaşı, Selen

Yüksek Lisans, Makina Mühendisliği Bölümü

Tez Yöneticisi : Doç. Dr. E. İlhan Konukseven

Ortak Tez Yöneticisi : Dr. Orhan Gülcan

Kasım 2018 , 84 sayfa

Titanyum ve alaşımları mekanik malzeme özellikleri sayesinde sanayinin birçok alanında tercih edilmektedir. Korozyon dayanıklılığı, yüksek mukavemet dayanımı ve düşük yoğunluk gibi iyi özelliklerinin yanında ham madde tedarik sürelerinin uzunluğu, işlenebilirliğinin zor ve maliyetli olması titanyum kullanımını sınırlandırmaktadır. Diğer yandan gelişen katmanlı imalat yöntemleri sayesinde karmaşık parçaların toz hammaddeden üretimi mümkün hale gelmiş ve günümüz araştırmaları bu yeni teknolojiler üzerinde yoğunlaşmaktadır.

Katmanlı imalat yöntemlerinden biri olan “Elektron Işını ile Ergitme” tasarımcılara geleneksel yöntemlerle üretilmiş parçaların malzeme özellikleri ile rekabet edebilecek, optimize edilmiş karmaşık parçaları geliştirmeleri konusunda olanak tanımaktadır.

Bu tez çalışmasının ilk aşamasında elektron ışını ile ergitme yöntemi kullanılarak ASTM E8 standardına uygun olarak dokuz adet numune farklı kurulum yönlerinde (makine çalışma koordinatlarına göre X, Y ve Z yönlerinde) üretilmiştir. Yüzey pürüzlülüğünün mekanik özellikler üzerindeki etkisinin görülmesi amacıyla, her yönde üretilen birer numune tornalama işlemine tabii tutulmuştur. Daha sonra her bir numune çekme testi uygulanmış, yüzey pürüzlülüğü ölçülmüş ve kırılma yüzeyleri mikroskobik ortamda incelenmiştir. Sonuç olarak dikey olarak üretilen parçaların çekme özelliklerinin daha iyi olduğu gözlemlenmiştir.

Çalışmanın ikinci aşamasında, aynı çalışma fonksiyonuna sahip daha hafif, karmaşık yapıların katmanlı imalat ile üretiminin mümkün olduğunu göstermek amacıyla, testlerle elde edilen veriler kullanılarak örnek bir uçak parçasının topoloji optimizasyonu yapılmıştır. Parça yatay ve dikey olarak üretilmek üzere iki adet optimizasyona tabii tutulmuştur. Parçanın konumlandırılması, yük koşulları ve karşılık gelen gerilim değerlerine göre belirlenmiştir. Optimizasyon sonucunda sistem performansında kayıp yaşamadan, yaklaşık olarak %40 daha hafif tasarımlar elde edilmiştir.

Anahtar Kelimeler: Katmanlı İmalat, Elektron Işını ile Ergitme, kurulum yönü, çekme özellikleri, Ti6Al4V, topoloji optimizasyonu, parça yerleşimi



To my love Cihan,  
and my lovely daughter Bade

## **ACKNOWLEDGMENTS**

I would like to express my sincere gratitude to my supervisor Assoc. Prof Dr. Erhan İlhan Konukseven for his patience and guidance throughout this study. I should also thank him for showing me the support and understanding while I was managing my job and the thesis together.

I would like to thank my co-supervisor Dr. Orhan Gülcan for his invaluable feedback, supervision and guidance on the research.

There are many people who helped throughout the study and it is impossible to list them name by name here. I am very grateful for the contribution of each and every colleague in the business.

I would like to thank my family members, especially to my mother Nurcan Ergül and my brother Mertcan Temel, for their support and for reminding me how lucky I am.

I owe the biggest thanks to Cihan Yiğitbaşı. I could not succeed without his help, encouragement and love.

And my lovely daughter Bade. I could not find the power to finish this work without your existence. We are looking forward for you to come impatiently.

## TABLE OF CONTENTS

ABSTRACT . . . . .	v
ÖZ . . . . .	vii
ACKNOWLEDGMENTS . . . . .	x
TABLE OF CONTENTS . . . . .	xi
LIST OF TABLES . . . . .	xv
LIST OF FIGURES . . . . .	xvii
LIST OF ABBREVIATIONS . . . . .	xxii
CHAPTERS	
1 INTRODUCTION . . . . .	1
1.1 Thesis Purpose . . . . .	2
1.2 Literature Survey . . . . .	2
1.3 Scope . . . . .	10
2 METALLIC ADDITIVE MANUFACTURING . . . . .	13

2.1	Examples of Current Technologies for Metallic Additive Manufacturing Techniques . . . . .	13
2.2	Electron Beam Melting . . . . .	15
2.2.1	Machine Layout, Components and Characterization of EBM Process . . . . .	16
2.2.2	Process Parameters . . . . .	18
2.2.3	Advantages of EBM . . . . .	20
2.2.4	Disadvantages and Limitations . . . . .	20
3	STRUCTURAL OPTIMIZATION . . . . .	23
3.1	Structural Optimization Methods . . . . .	23
3.1.1	Sizing Optimization . . . . .	23
3.1.2	Shape Optimization . . . . .	24
3.1.3	Topology Optimization . . . . .	24
3.2	Method of Topology Optimization . . . . .	24
3.3	Finite Element Method . . . . .	25
3.4	Software Usage for Topology Optimization . . . . .	26
3.4.1	Optistruct . . . . .	26
3.4.2	Topology Optimization with Optistruct . . . . .	26
4	EXPERIMENTAL STUDY . . . . .	29

4.1	Experimental Procedure . . . . .	29
4.2	Manufacturing of the Samples . . . . .	29
4.2.1	Properties of the Samples . . . . .	29
4.2.2	Process Parameters . . . . .	30
4.2.3	Samples Built by EBM . . . . .	34
4.2.4	Post Process . . . . .	35
4.3	Tensile Test . . . . .	36
4.3.1	Mechanical Properties of the Samples Built by EBM	36
4.3.2	Comparison of the Results with Cast and Wrought Material Properties . . . . .	44
4.4	Surface Roughness Tests for Samples . . . . .	46
4.5	Fracture Surface Analysis . . . . .	48
4.6	Microstructure . . . . .	51
5	TOPOLOGY OPTIMIZATION OF AN AIRCRAFT FITTING . . . .	55
5.1	Optimization Model . . . . .	55
5.1.1	Finite Element Model . . . . .	57
5.1.2	Material and Property . . . . .	57
5.1.3	Load Collectors and Load Steps . . . . .	58
5.1.4	Static Analysis and Results . . . . .	59

5.2	Usage of the Properties Gained from Experiment . . . . .	60
5.3	Optimization Steps . . . . .	63
5.3.1	Design and Non-Design Spaces . . . . .	63
5.3.2	Finite Element Model . . . . .	64
5.3.3	Material and Property . . . . .	65
5.3.4	Load collectors and Load Steps . . . . .	65
5.3.5	Optimization parameters . . . . .	65
5.3.6	Optimization Results . . . . .	67
5.3.7	CAD Models after Optimization . . . . .	70
5.3.8	Stress Analysis for the Final Models . . . . .	70
5.4	Comparison of the Main Design and Optimized Models . . .	74
6	CONCLUSION AND FUTURE WORK . . . . .	77
	REFERENCES . . . . .	79

## LIST OF TABLES

### TABLES

Table 1.1	Tensile properties of the specimens produced by EBM from Edwards et al. study . . . . .	4
Table 1.2	Process parameters used for SLM from Gong et al. study . . . . .	5
Table 1.3	Process parameters used for EBM from Gong et al. study . . . . .	5
Table 1.4	Tensile properties of the related samples from Gong et al. study . .	6
Table 2.1	Summary of the characteristics of Q20 EBM machine . . . . .	18
Table 4.1	Chemical composition of the ARCAM Ti6Al4V powder . . . . .	30
Table 4.2	Process parameters for preheat operation . . . . .	31
Table 4.3	Process parameters for melt operation . . . . .	32
Table 4.4	Process parameters for wafer operation . . . . .	32
Table 4.5	Process parameters for net operation . . . . .	33
Table 4.6	Tensile properties of the specimens . . . . .	43
Table 4.7	Comparison of the results by building direction . . . . .	43
Table 4.8	Comparison of chemical properties of the ARCAM Ti6Al4V powder to cast and wrought Ti6Al4V materials . . . . .	45
Table 4.9	Comparison of mechanical properties of the tensile specimens with ARCAM Ti6Al4V powder, cast and wrought Ti6Al4V materials . . . . .	45

Table 4.10 $R_a$ and $R_z$ values of the tensile specimens . . . . .	47
Table 5.1 Loads according to analysis coordinate system . . . . .	59
Table 5.2 Static analysis results for the main design . . . . .	60
Table 5.3 Planar stress components at maximum von-mises stress location for critical load case . . . . .	61
Table 5.4 Static analysis results for the parts to be built horizontally . . . . .	72
Table 5.5 Static analysis results for the parts to be built vertically . . . . .	73



## LIST OF FIGURES

### FIGURES

Figure 1.1 Schematic of specimen orientation in machine from Edwards et al.'s study . . . . .	3
Figure 1.2 Geometry and building orientations for Formanoir et al. study . . .	4
Figure 1.3 Average tensile strength for each sample series used by Algardh et al. . . . .	6
Figure 1.4 Density plot and final model of optimized part . . . . .	7
Figure 1.5 Weight change in bracket design from Vasudeva Rao and Soundararajan's work . . . . .	8
Figure 1.6 Design space of engine mounting bracket used on Sreedhar and Sasidhar's study . . . . .	9
Figure 1.7 Optimization output and optimization based CAD model of Sreedhar and Sasidhar research . . . . .	9
Figure 1.8 Optimization example from Waltona and Moztarzadehb's paper . .	9
Figure 1.9 The as-built parts before support removal and post-machined EBM parts from Waltona and Moztarzadehb's work. . . . .	10
Figure 1.10 Optimization steps used in Marchesi et al.'s research . . . . .	11
Figure 1.11 A titanium part produced conventionally and optimized design according to additive manufacturing capabilities . . . . .	11
Figure 2.1 SLS machine layout and work principle . . . . .	13

Figure 2.2	The schematic of SLM work principle . . . . .	14
Figure 2.3	A basic schematic for EBFF technology . . . . .	15
Figure 2.4	Configuration of LMD . . . . .	15
Figure 2.5	The machine layout of WAAM . . . . .	16
Figure 2.6	EBM machine layout . . . . .	17
Figure 2.7	Scanning pattern for layer fabrication . . . . .	19
Figure 3.1	Examples for structural optimization . . . . .	23
Figure 4.1	Dimensions of the tensile test specimen according to ASTM E8M .	30
Figure 4.2	Building directions of the specimens and their locations in vacuum chamber according to machine coordinate system . . . . .	31
Figure 4.3	An example for layer by layer building process . . . . .	33
Figure 4.4	Side views of X and Y specimens with support geometries after manufacturing by EBM . . . . .	34
Figure 4.5	As-built Z specimen . . . . .	34
Figure 4.6	A sample of X and Y specimens after grinding operation . . . . .	35
Figure 4.7	Visual of a post machined specimen . . . . .	35
Figure 4.8	Tensile test setup . . . . .	36
Figure 4.9	X1 tensile stress vs. tensile strain graph . . . . .	37
Figure 4.10	X1 extension vs. load graph . . . . .	37
Figure 4.11	X2 tensile stress vs. tensile strain graph . . . . .	37
Figure 4.12	X2 extension vs. load graph . . . . .	38
Figure 4.13	X3 tensile stress vs. tensile strain graph . . . . .	38

Figure 4.14 X3 extension vs. load graph . . . . .	38
Figure 4.15 Y1 tensile stress vs. tensile strain graph . . . . .	39
Figure 4.16 Y1 extension vs. load graph . . . . .	39
Figure 4.17 Y2 tensile stress vs. tensile strain graph . . . . .	39
Figure 4.18 Y2 extension vs. load graph . . . . .	40
Figure 4.19 Y3 tensile stress vs. tensile strain graph . . . . .	40
Figure 4.20 Y3 extension vs. load graph . . . . .	40
Figure 4.21 Z1 tensile stress vs. tensile strain graph . . . . .	41
Figure 4.22 Z1 extension vs. load graph . . . . .	41
Figure 4.23 Z2 tensile stress vs. tensile strain graph . . . . .	41
Figure 4.24 Z2 extension vs. load graph . . . . .	42
Figure 4.25 Z3 tensile stress vs. tensile strain graph . . . . .	42
Figure 4.26 Z3 extension vs. load graph . . . . .	42
Figure 4.27 Mahr model surface tester . . . . .	46
Figure 4.28 ZEISS Sigma 300 Scanning Electron Microscope . . . . .	47
Figure 4.29 SEM pictures from the surfaces of as-built Z samples . . . . .	48
Figure 4.30 Stereo Zoom Microscope setup . . . . .	48
Figure 4.31 Fracture surfaces of specimens . . . . .	49
Figure 4.32 Visuals of machined and as-built parts after tensile test . . . . .	50
Figure 4.33 SEM pictures of the fracture surfaces of the specimens . . . . .	50
Figure 4.34 SEM picture of the fracture surface of machined X specimen . . . . .	51
Figure 4.35 Metkon Ecoperss 50 Mounting Press . . . . .	52

Figure 4.36 Buehler Beta Grinder-Polisher . . . . .	52
Figure 4.37 Leica DM2700 M Optical Microscope . . . . .	53
Figure 4.38 Microstructure of X and Y specimens . . . . .	53
Figure 4.39 Microstructure of Z specimen . . . . .	54
Figure 5.1 An aircraft fitting . . . . .	56
Figure 5.2 Views of the assembly of the fitting to be optimized . . . . .	56
Figure 5.3 FEM model on Altair Hyperworks . . . . .	57
Figure 5.4 Material view on Altair Hyperworks . . . . .	58
Figure 5.5 Property panel view on Altair Hyperworks . . . . .	58
Figure 5.6 First load step creation on Hyperworks . . . . .	59
Figure 5.7 Hypermesh view for the first load case . . . . .	60
Figure 5.8 Maximum von-mises stresses plot for load case 1 on Hyperview . .	61
Figure 5.9 Direction of resultant stress component at XZ plane according to analysis coordinate system . . . . .	62
Figure 5.10 Desired locations for the vertical and horizontal parts according to machine/work coordinate system . . . . .	63
Figure 5.11 Design and non-design spaces . . . . .	64
Figure 5.12 FEM model of optimization model on Hypermesh . . . . .	64
Figure 5.13 Optimization panel on Optistruct . . . . .	65
Figure 5.14 Design variable parameters screen for minimum member size con- trol and stress constraint . . . . .	66
Figure 5.15 Design variable pattern grouping screen for symmetry definition .	67
Figure 5.16 Creation of the virtual plane for one plane symmetry as pattern type	67

Figure 5.17 Contour plot for optimization results for the part oriented horizontally	68
Figure 5.18 Optimization model of the horizontal part for 0.3 iso density value .	68
Figure 5.19 Contour plot of optimization results for the part oriented vertically .	69
Figure 5.20 Optimization model of the vertical part for 0.35 iso density value .	69
Figure 5.21 Last optimized model for the horizontal part with smooth surfaces .	70
Figure 5.22 Last optimized model for vertical part with smooth surfaces . . . .	71
Figure 5.23 Hypermesh view for first load case . . . . .	71
Figure 5.24 Results of the first load case for horizontal part . . . . .	72
Figure 5.25 Results of the first load case for vertical part . . . . .	73
Figure 5.26 Comparison of the main design and optimization models . . . . .	74
Figure 5.27 As-built vertical optimization part . . . . .	74

## **LIST OF ABBREVIATIONS**

Ti	Titanium
Al	Aluminum
V	Vanadium
C	Carbon
Fe	Iron
O	Oxygen
N	Nitrogen
H	Hydrogen
FEM	Finite Element Method
FEA	Finite Element Analysis
2D	Two Dimensional
3D	Three Dimensional
CAD	Computer Aided Design
RPM	Revolution per Minute
DOF	Degree of Freedom
EBM	Electron Beam Melting
AM	Additive Manufacturing
SEM	Scanning Electron Microscope
ASTM	American Society for Testing and Materials
SLM	Selective Laser Melting
SLS	Selective Laser Sintering
DMLS	Direct Metal Laser Sintering
EBFF	Electron Beam Freeform Fabrication

LMD	Laser Metal Deposition
WAAM	Wire Arc Additive Manufacturing
UTS	Ultimate Tensile Strength
YS	Yield Strength
E	Elastic of Modulus
RF	Reserve Factor





## **CHAPTER 1**

### **INTRODUCTION**

Additive manufacturing (AM) has an important role in today's industry since it provides shorter design cycles, low cost and flexible products. While AM techniques focused on only modeling and prototyping past years, with developing technology, manufacturing rapid tooling such as casting molds has been included in the scope of AM [1, 2]. Today, it is possible to manufacture nearly end use parts with improvements in technology and used materials. On the other hand, it is not always possible to produce low cost, effective parts by AM. It depends on the complexity, material and production rates.

Titanium (Ti) and its alloys are preferred materials to use in automotive, dental and aerospace applications because of their high strength, low density and high corrosion resistance characteristic. However, long lead times, machining restrictions and high costs in traditional methods restrict usage area of those materials. At this point, AM seems a good option for producing of Ti parts.

Electron Beam Melting (EBM), an AM technique, was invented by ARCAM Company to produce complex metallic parts that have comparable properties to the ones produced by conventional manufacturing methods. The machine uses metallic powder as raw material and builds parts layer by layer to the desired geometry. Therefore, EBM has a good potential to produce complex Ti parts with lower lead times and design cycles. But mechanical properties of the end parts depend on the process parameters of the machine. Therefore, EBM researches focus on the effects of process parameters.

Related researches show that different building directions directly affect the final mechanical properties that depend on the metallurgical bonding of two neighbor melt tracks and layers. Slicing each layer parallel or perpendicular to direction of the load

affects grain arrangements and the tensile properties [3], [4]. In this study, building direction effect is examined while other parameters remain the same according to the company recommendations.

AM gives an opportunity to designers to be flexible at designing stage. It is possible to have lighter parts with complexity which is very critical for aerospace industry. At this point optimization methods are met with the AM researches. Topology optimization, for example, is used to design conceptual structural parts with mass reduction object. But in general, optimization results cannot be used directly with traditional manufacture processes [5]. Thanks to the layer by layer building process of AM that decrease the limitations on design, topology optimization is utilized for direct manufacturing. In this study, topology optimization is conducted according to the experimental data of the parts produced by EBM. It is aimed to mix AM and topology optimization studies to show that it is possible to manufacture complex parts with weight reduction.

## **1.1 Thesis Purpose**

The main purpose of this study is to investigate the mechanical properties of Ti6Al4V parts manufactured by EBM and to see the effect of building direction on those properties. The study also aims to show that it is possible to design lighter parts by topology optimization without loss on working function of the component by additive manufacturing and to see the effect of building direction on optimization results.

## **1.2 Literature Survey**

Literature survey of the thesis consists of two parts; mechanical properties of Ti6Al4V produced by AM and topology optimization studies.

Hrabe and Quinn investigated the effects of orientation on mechanical properties of Ti6Al4V fabricated by EBM. Their results revealed that the reported values of ultimate tensile strength (UTS) and yield strength (YS) remain unaffected by orientation (UTS: 1017-1030 MPa in X-Y, 1009-1033 MPa in Z, YS: 967-983 MPa in X-Y, 961-984 MPa in Z) but elongation is 30% higher in the X-Y direction (12.2% in X-Y,

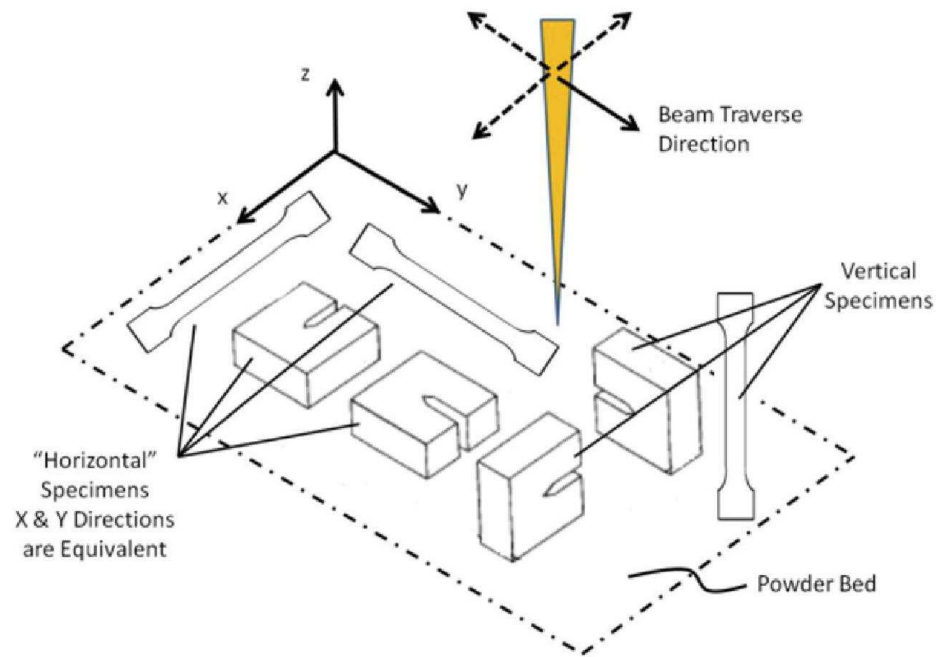


Figure 1.1: Schematic of specimen orientation in machine from Edwards et al.'s study [4]

7.0-9.0% in Z) [3].

Edwards et al. investigates the fatigue properties of Ti6Al4V specimens and components produced by EBM with ARCAM A1 Machine. Five horizontal oriented and five vertical oriented specimens have been built with 6x20x200mm in dimensions as shown in Figure 1.1. They changed power from 50 to 3500W, and used spot size of 0.2–1.0mm and a beam speed of 3m/s as input parameters. The process was conducted in a vacuum chamber at 700°C. No heat treatment was performed after building of samples. The results of the tests are shown in Table 1.1. In both orientations, the strength and elongations are lower than handbook values for wrought Ti6Al4V [6] and other published studies [7], [8] on the static properties of AM Ti materials. To decrease residual stress during solidification and cooling of the melted layers and not to perform stress relief post process, the manufacturing was done at the elevated temperature in the build chamber. But, they stated that if the concern is porosity or fatigue life, stress relief heat treatment is still required [4].

Zhai et al. compared Ti6Al4V parts produced by Laser Engineered Net Shaped (LENS) and EBM. They used two different laser power as input parameter (330 W, 780 W). For LENS parts, as the laser power increased, YS and UTS of the LENS

Table 1.1: Tensile properties of the specimens produced by EBM from Edwards et al. study [4]

	UTS (MPa)		0.2% YS (MPa)		Elongation %	
Orientation	Ave	Stdev	Ave	Stdev	Ave	Stdev
Horizontal	833	22	783	15	2.7	0.4
Vertical	851	19	812	12	3.6	0.9

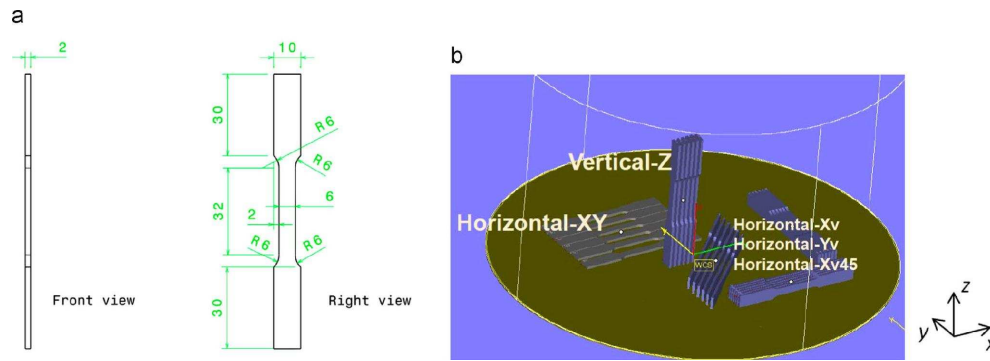


Figure 1.2: **a)** Geometry of the specimen (dimensions are in mm) **b)** building orientations for Formanoir et al. study [10]

produced parts changed from 1005-1103 MPa and 990-1042 MPa, respectively. For vertical EBM parts from 1001-1051 MPa and 1073-1116 MPa, respectively, for horizontally orientated EBM parts, those changed from 973-1006 MPa and 1032-1066 MPa, respectively. It is concluded that when building orientation changed from horizontal to vertical, tensile direction changed and YS and UTS increased [9].

Formanoir et al., examined the past studies in literature. They noted that very large range of tensile properties is reported in papers with YS levels changing from 780MPa to 1130MPa and strains changing from 2.3% to 20%. Examined tensile specimens and their building orientations are shown in Figure 1.2. Some of the specimens were mechanically polished after building, to show effect of surface roughness on the mechanical properties. As-built parts resulted with  $832 \pm 24$  MPa YS and a strain to failure of  $3.64 \pm 1.2\%$ . And the polished parts resulted with  $1055 \pm 11.5$  Mpa and  $4.58 \pm 0.78\%$  respectively. Polished specimens resulted with higher strain to failure related the porosity. In this study heat treatment after building was also examined and it was shown that it does not have huge effect on mechanical properties [10].

The effect of building direction on mechanical properties of AM lattice structures was investigated by Wauthle et al. They concluded that the compressive strength and the

Table 1.2: Process parameters used for SLM from Gong et al. study [13]

Parameter No	Scan Speed (mm/s)	Energy Density (J/mm <sup>3</sup> )
SLM-1	960	42
SLM-2	540	74
SLM-3	400	100
SLM-4	1260	32
SLM-5	1500	27

Table 1.3: Process parameters used for EBM from Gong et al. study [13]

Parameter No	Max Current (mA)	Speed Function Index	Line Offset (mm)	Focus Offset (mm)
EBM-1	21	98	0.1	3
EBM-2	30	60	0.2	15
EBM-3	20	180	0.2	5

stiffness of the 45° oriented sample are 35% lower on average compared to the vertically positioned sample that has almost the same properties with horizontal sample [11].

The effect of building direction on the fatigue performance of Ti6Al4V was investigated by Wycisk et al. They found no significant difference between building direction of 45° and 90° to the base plate in the fatigue performance [12].

The study of Gong et al. contains the comparison of the mechanical properties of Ti6Al4V samples produced by Selective Laser Melting (SLM) and EBM. Different process parameters were used to produce samples shown in Table 1.2 and Table 1.3. For SLM, 120W laser power, 0.1mm hatch spacing and 0.03mm layer thickness were used for all cases. For EBM, 0.05mm layer thickness was used as common for all the cases. Mechanical properties of the samples are also shown in Table 1.4 [13].

The study of Al-Bermani et al. revealed that the mechanical properties of Ti6Al4V parts produced by EBM as 993.9-1031.9 MPa UTS, 883.7-938.5 MPa YS and 11.6-13.6% elongation [14].

Carroll et al. investigated the tensile behavior of Ti6Al4V components fabricated with directed energy deposition. They used 2000 W laser power and 10.6 mm/s scanning velocity for all specimens. They concluded that the YS and UTS values for all AM specimens of  $959 \pm 22$  and  $1064 \pm 23$  MPa, respectively. They are close to the wrought baseplate values of  $973 \pm 8$  and  $1050 \pm 8$  MPa [15].

Table 1.4: Tensile properties of the related samples from Gong et al. study [13]

Parameter No	0.2% Proof Stress (MPa)	UTS (MPa)	Elongation (%)	Young's Modulus (GPa)
SLM-1	1098	1237	8.8	109
SLM-2	1150	1257	8.0	111
SLM-3	1066	1148	5.4	109
SLM-4	932	1112	6.6	95
SLM-5	813	978	3.7	84
EBM-1	962	1012	8.8	121
EBM-2	947	1011	9.0	120
EBM-3	-	423	0.4	92

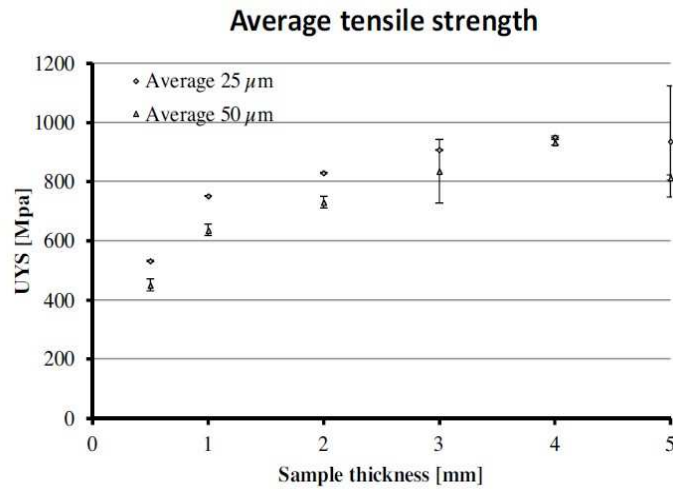


Figure 1.3: Average tensile strength for each sample series used by Algardh et al. [17]

In their study, Wang et al. used Ti6Al4V powders with 30-50  $\mu\text{m}$  diameter to build a part by EBM process. They used 70  $\mu\text{m}$  layer thickness and worked with four different scanning speeds (214 mm/s, 376 mm/s, 529 mm/s and 689 mm/s). They concluded that the Young's modulus (E) of the produced parts is around 111.7 ~ 119.0 GPa, which are comparable to the wrought Ti6Al4V. The study concludes that as the beam scanning speeds increase, the Young's modulus and also hardness increase due to finer microstructure [16].

Algardh et al. studied the effect of powder size on tensile properties of Ti6Al4V parts produced by EBM. They used powder size around 25  $\mu\text{m}$  and 50  $\mu\text{m}$ . The findings show that microstructure is dependent on wall-thickness. For thin walled structures, tensile properties can become dominant according to variations in surface roughness.



Figure 1.4: **(a)** Uniform density plot of the component, **(b)** Final optimized model of Viqaruddin et al. study [21]

The change in tensile strength can be shown in the Figure 1.3 [17].

Since it has a direct effect on mechanical properties, it is important to measure the elemental composition of recycled powder. In their study on powder recycling of Ti6Al4V in EBM, Tang et al. showed that aluminum content decreased from 6.47 to 6.37%, vanadium decreased from 4.08 to 4.03% and oxygen increased from 0.08 to 0.19% by weight after 21 reuse cycles. According to study, YS and UTS increased since oxygen content was increased with reuse cycles. Also, elongation was unaffected by oxygen content. Those results show that, mechanical properties are not affected negatively with powder recycling [18].

Edwards et al. noted that the mechanical properties of machined parts might be higher than those of as-built parts at EBM technology. Especially, when fatigue properties are considered it is important to choose dimensions accordingly [19].

The main advantage of the additive manufacturing is its capacity to manufacture complex geometry, so the flexibility for design. As Antonysamy et al. mentioned in their study with EBM technology, it also provides an opportunity to decrease ratio between the weight of the raw material and the actual weight of the design [20]. With flexibility of designing part, it is also possible to manufacture lighter parts without changing performance of the component. For this purpose, optimization methods can be used. Viqaruddin et al. used the topology optimization approach in their study for an aluminum engine mount bracket. By using structural optimization method with Hyperworks, a commercial product, they had resulted 41% weight reduction without varying performance of the component. Density plot and final model can be seen on Figure 1.4 [21].

Vasudeva Rao and Soundararajan worked on optimization of vibration characteristics

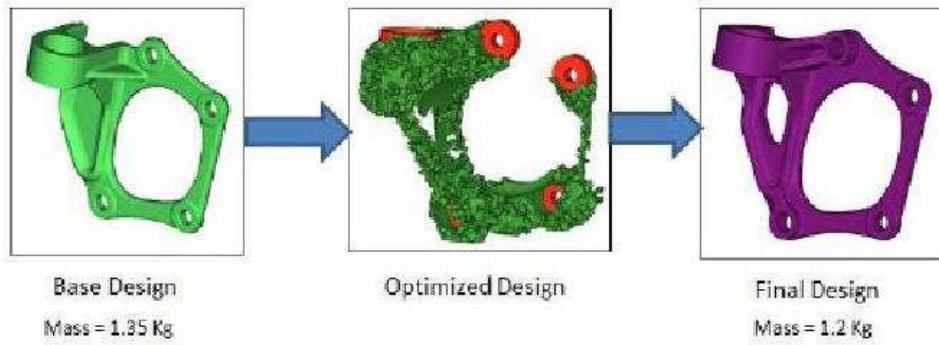


Figure 1.5: Weight change in bracket design from Vasudeva Rao and Soundararajan's work [22]

of a bracket. In their study, a driveline was used for speed and torque transfer and for vibration isolation, bracket attachments were used to get the dynamic stiffness. To determine natural frequencies, modal analysis was done. Objective function is determined as to maximize the frequency by introducing stiffeners at more strain energy location to the bracket. Even though it was not the main purpose, design weight also decreased from 1.35 kg to 1.2kg [22].

Sreedhar and Sasidhar studied on topology optimization of an engine mounting bracket shown in Figure 1.6. The system contains an engine, a foundation and three to four engine mounts. Due to vibration occur in the system, it is needed to be properly constrained and isolated. The purpose of the optimization is to minimize the volume without effect the stiffness and strength of the bracket. After optimization and re-design process final design can be seen in Figure 1.7, the weight was reduced by 20% as fatigue and strength properties met the requirements and frequency and stiffness values were improved [23].

Waltona and Moztarzadehb's paper examines a design and development process for EBM with topology optimization. Study contains EBM design principles and mechanical properties validation for Ti6Al4V. With purpose of weight reduction, parts were redesigned and manufactured by EBM. Also EBM part yielded an 86% reduction in raw material use [24]

The study concludes that, EBM can help produce functional components with almost unlimited geometry capabilities by using topology optimization methods. To minimize support structures, shape controls during topology optimization can be done.



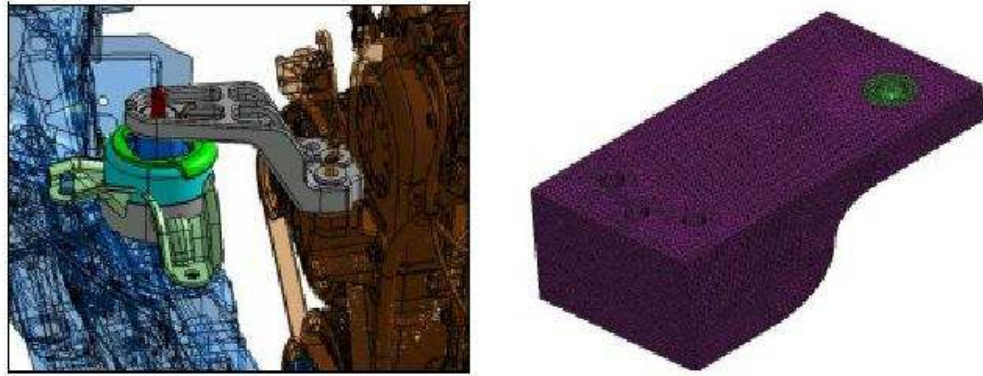


Figure 1.6: Design space of engine mounting bracket used on Sreedhar and Sasidhar's study [23]

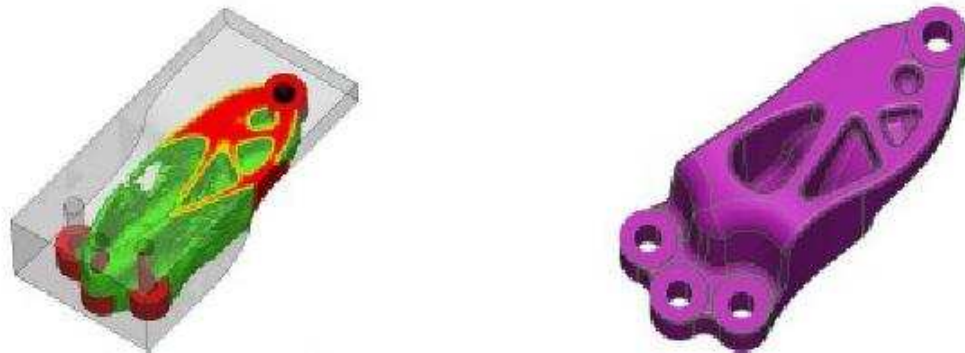


Figure 1.7: Optimization output and optimization based CAD model of Sreedhar and Sasidhar research [23]

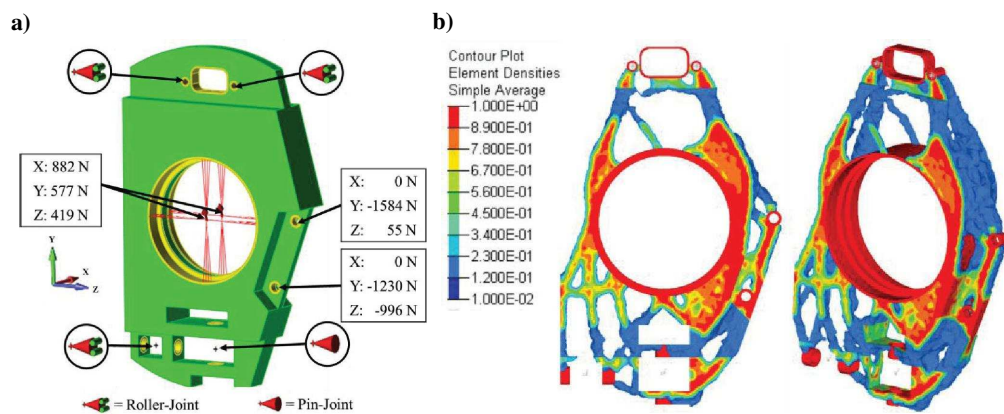


Figure 1.8: **a)** The design space and loading conditions on the rear upright. **(b)** Post optimization result from Waltona and Moztarzadehb's paper [24]

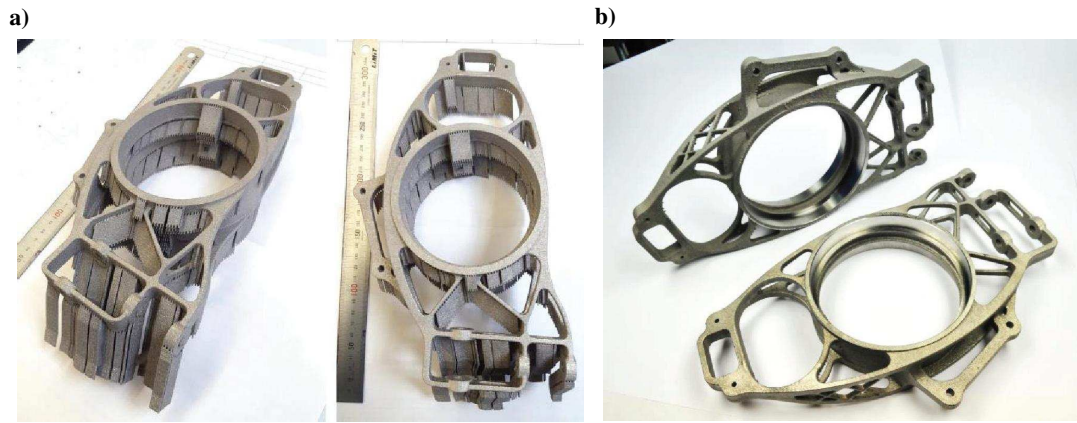


Figure 1.9: **(a)** The as-built parts before support removal. **(b)** The post-machined EBM parts from Waltona and Moztarzadehb's work. [24]

This helps to reduce time and cost. Using a fully parameterized model with topology optimization allows for a simpler redesign process as using EBM design guidelines and rules [24].

Marchesi et al. optimized a diesel engine topologically to manufacture by an AM method in their study. In their optimization two function were taken in consideration; connection between the powertrain and the main body of the vehicle, and anchor for a pulley that enforces tension to the belt. The optimization steps can be shown in Figure 1.10. This study emphasis on the combination of topological optimization and additive manufacturing has great potential to replace traditional design and manufacturing processes [25].

Another example of a machined part and optimized version can be seen on Figure 1.11. The visuals were taken from Edwards et al.'s paper that was mentioned in the beginning of this section [4].

### 1.3 Scope

The scope of the thesis is to investigate mechanical properties of the parts manufactured by EBM. Only the building direction effect was examined and all other process parameters were remained the same as company recommendation through study. The study also covers topology optimization of an aircraft fitting according to experimental data. Optimization was done via Hyperworks Optistruct tool and mathematics of

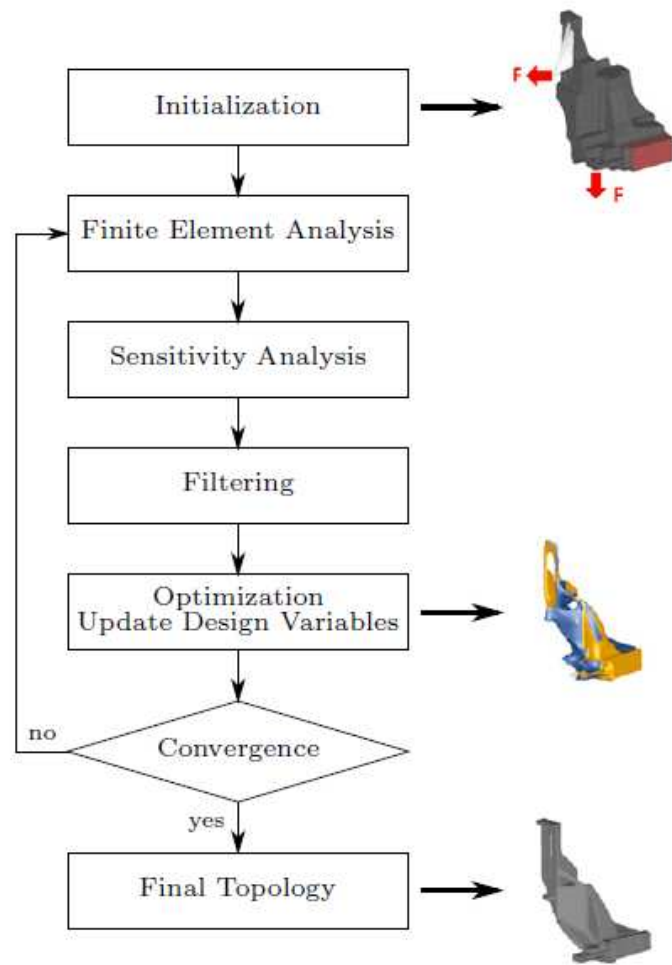


Figure 1.10: Optimization steps used in Marchesi et al.'s research [25]

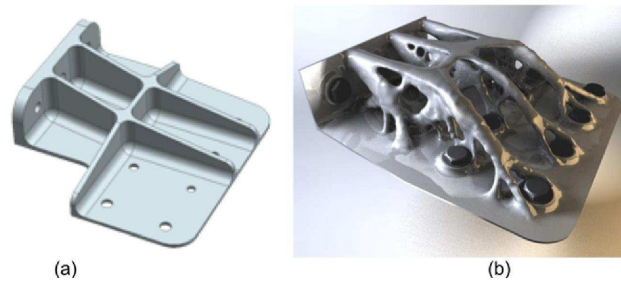


Figure 1.11: **a)** A titanium part produced conventionally. **(b)** Optimized design according to additive manufacturing build capabilities [4].

the optimization method is not in the scope of this study. Model, boundary conditions, loads and limitations on optimization (see Section 5.3.1) were predefined and derivation of them is not covered through this thesis.

## CHAPTER 2

### METALLIC ADDITIVE MANUFACTURING

#### 2.1 Examples of Current Technologies for Metallic Additive Manufacturing Techniques

Metal AM Techniques can be divided into two groups: Powder Bed Technologies and Direct Deposition Technologies according to raw material's usage technique. EBM and SLM are in the group of Powder Bed AM Techniques and fabricate parts by melting powders. Selective Laser Sintering Technology (SLS) is also in this group and fabricates parts by sintering powders by a laser.

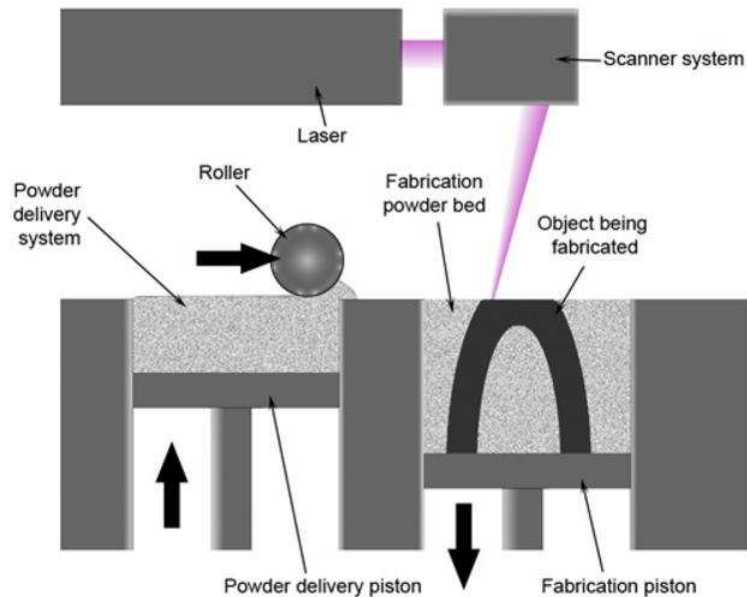


Figure 2.1: SLS machine layout and work principle [26]

In SLS technology, powders of ceramic, plastic or glass are sintered to fuse powder together by a laser. Figure 2.1 illustrates the machine layout and how it works. Direct

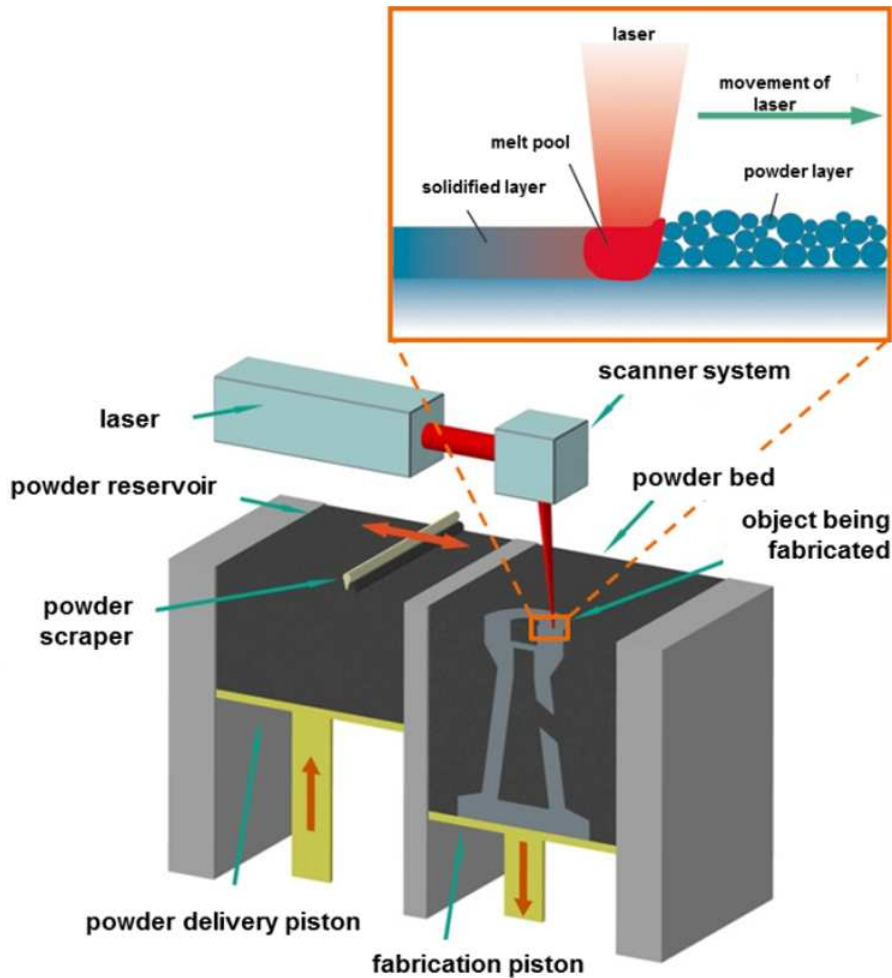


Figure 2.2: The schematic of SLM work principle [27]

Metal Laser Sintering (DMLS) works with the same procedure but with metal alloys used as raw material.

SLM uses metal powder such as stainless steel and titanium and melts the powder locally by a laser. Different from DMLS, laser is used to achieve a full melt, other than sintering. Working principle of the SLM technology can be seen on Figure 2.2. For Direct Deposition Methods, Electron Beam Freeform Fabrication (EBFF) can be shown as an example that melts the metallic wire by an electron beam to create each layer of the desired geometry.

Laser Metal Deposition (LMD) is also in Direct Deposition group and uses a laser beam to melt metal powder that is injected by a gas stream as seen in Figure 2.4.

Wire Arc Additive Manufacturing Technique (WAAM) is another example for Direct Deposition Technologies that consists a welding torch as heat source to melt the

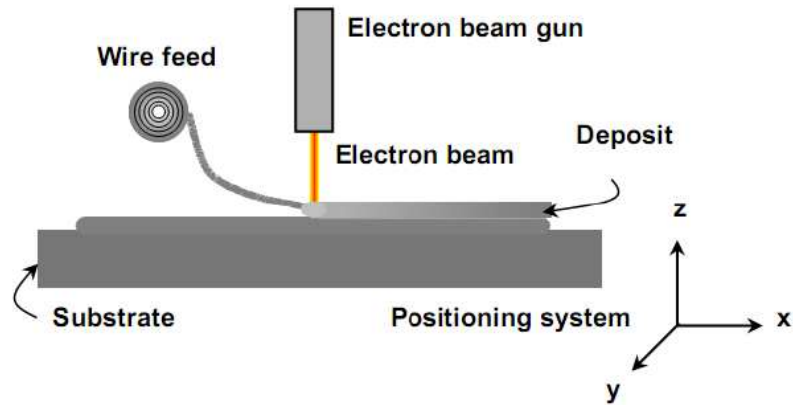


Figure 2.3: A basic schematic for EBFF technology [28]

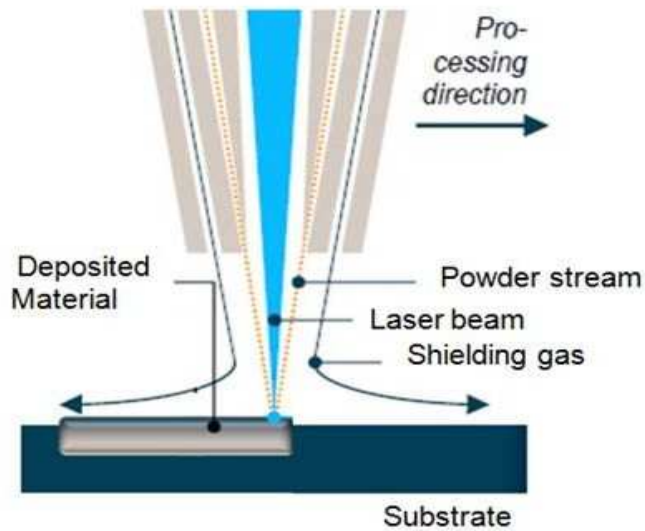


Figure 2.4: Configuration of LMD [29]

metallic wire. WAAM is not a exact shape process since layer height is in the range of 1-2mm, and this cause a high surface roughness [30]. Layout of the WAAM can be seen in Figure 2.5.

## 2.2 Electron Beam Melting

EBM, a powder bed AM technology, was invented by ARCAM Company located in Sweden. EBM was invented to manufacture the challenging designs such as complex aerospace structural parts or turbine blades that have comparable properties to the



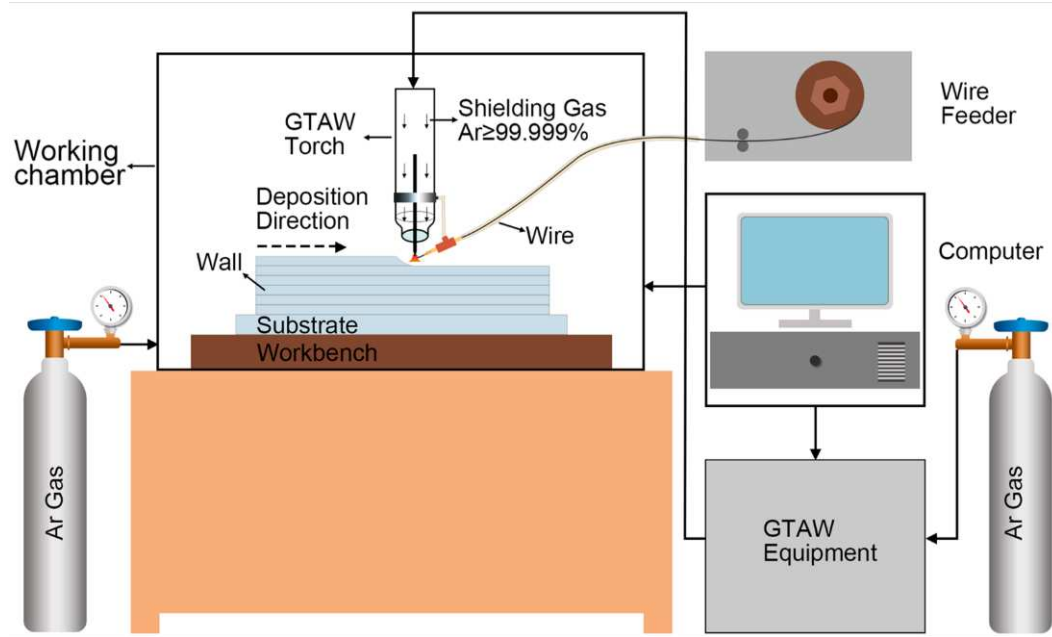


Figure 2.5: The machine layout of WAAM [31]

parts built by traditional methods with cast or wrought material.

In this section working principle, basic components and parameters of EBM are described.

### 2.2.1 Machine Layout, Components and Characterization of EBM Process

In this thesis, ARCAM Q20 EBM Machine is used. Layout of the machine can be seen on Figure 2.6 and general properties of the machine are summarized in Table 2.1.

As seen in the Figure 2.6, EBM has a vacuum chamber which contains two powder hoppers to dispense powder with a rake system to spread powder and building tank with adjustable building platform to manufacture part layer by layer. By heating tungsten filament electron beam is generated. By using lenses, electrons are focused and deflected. By hitting the powders on certain layer, electrons release the kinetic energy to melt powder particle for each layer.

The process begins with spreading a layer of powder on build chamber. With a relative low beam current and relative high scan speed “preheating” process takes place to sinter metal powder to get together loosely. Then, current layer is scanned by electron



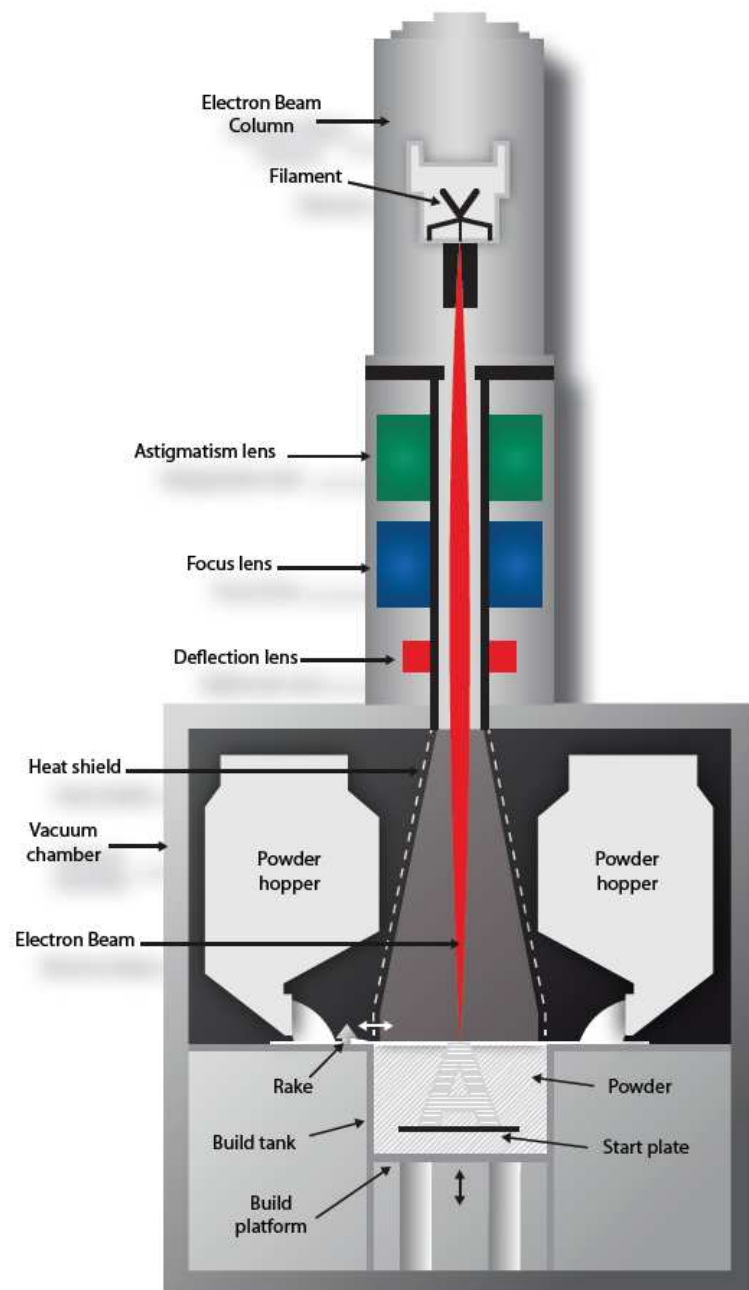


Figure 2.6: EBM machine layout [32]

Table 2.1: Summary of the characteristics of Q20 EBM machine

Size (WxDxH)	App. 2300x1300x2600 mm
Weight	2900 kg
Power Supply	3x400 V, 32 A, 7kW
Max. Build Size (Diameter/Height)	350x380mm
Max. Beam Power	3000W
Min. Beam Diameter	180 $\mu$ m
Repositioning Time	10ms
Vacuum Base Pressure	$1 \times 10^{-4}$ mbar
Build Atmosphere	$1 \times 10^{-3}$ mbar, partial pressure of He
He consumption, build process	4 l/h
He consumption, build cool down	100-150 l/build
Translation speed, melting	Continuously variable

beam and is melted to desired shape from a lightly joined powder layer to a compact layer with “melting” process. Support geometries are formed by “wafer” process and lastly, if there are lattice structure geometries, “net” process takes place. After current layer operations are finished, build platform moves down by layer thickness and the procedure is repeated until part is manufactured completely. When building of the part is done, cooling operation takes place under helium flow or vacuum.

### 2.2.2 Process Parameters

In this thesis, predefined process parameters given by the supplier as an algorithm were used. Summarized definitions of the main parameters are as follows:

#### Layer Thickness

As in other AM technologies, layer thickness is one of the main process parameters of EBM. It depends on powder size and has direct effect on quality of the part geometry.

#### Contour, Hatch and Line Offset

Each layer is formed by a scanning pattern formed by contours and hatches. Inner and outer boundaries of the part geometry are formed by contours. To fill the profile shape, lines called as hatch are followed up through contours. And distance between the hatches is known as line offset.

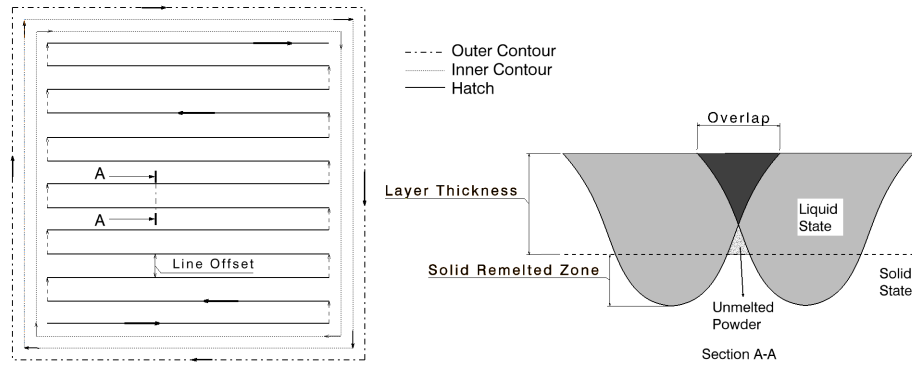


Figure 2.7: Scanning pattern for layer fabrication. (Arrows show the scan line direction.)

Line offset is also called as overlap and related to providing better surface quality. If the value of overlap is not sufficient, powder cannot fuse together adequately. If line offset is increased, overlap area decreases and unmelted powder may occur inside the part. (See Figure 2.7)

### Beam Current

Beam current is the input energy for the process, and current selection is directly depend on geometry. While lower values are used for thin structures, higher values are used for larger melt areas.

### Speed Factor

It is also called as speed function index. This parameter is a combined function of beam current and beam speed. It is related to energy input of the process, and used to control melt pool size. Speed Factor values are predefined by ARCAM build theme.

### Focus Offset

This is another process variable that is offset from its zero position to focus plane. This process parameter has a direct effect on energy density and beam diameter. As focus offset increases, energy density and melting depth decrease.

### Preheating Temperature

While creating layers, the powder particles are pushed away easily due to high energy

generation of the beam. In addition to the powder blown problem, the spheroidization shows up if powder temperature around melt pool is too low. To solve those problems and to gain better microstructure and mechanical properties, preheating process takes place in EBM method [33].

Preheating temperature provides the heating of metal powder close to the main melting temperature.

Process parameters used in this study are indicated in Section 4.2.2.

### **2.2.3 Advantages of EBM**

- Tooling needs (such as fixtures) are low or none.
- Complex geometries are possible to produce that are almost impossible or hard to produce by traditional methods such as lattice structures.
- It is more energy efficient technology compared to laser additive manufacturing technology.
- For prototype manufacturing, it is a cost and time saving technology.
- EBM has low material waste compared to traditional methods.
- Low residual stresses occur through processes because of the preheating strategy.

### **2.2.4 Disadvantages and Limitations**

- It is expensive compared to traditional methods.
- Porosity and surface quality are main concerns through processes. EBM process cause rough surface finish compared to some other metallic AM techniques such as SLM.
- Minimum beam diameter is an important constraint for building thin and lattice geometries.
- For complex parts, wafer supports are needed. It causes warping on part geometry because of the thermal expansions through processes.

- In some cases, it is hard to remove support geometries and for surface quality post machining is a must.
- The preparing and post processes for the machine is too long, and significant amount of validation is needed for the EBM process.
- Preventative maintenance is required for the machine.
- Lead time for the powder material and other equipments needed for the process is long due to limited supply chain.



## CHAPTER 3

### STRUCTURAL OPTIMIZATION

#### 3.1 Structural Optimization Methods

According to geometric feature of the structure, structural optimization problems can be divided into three groups: Sizing, shape and topology optimization.

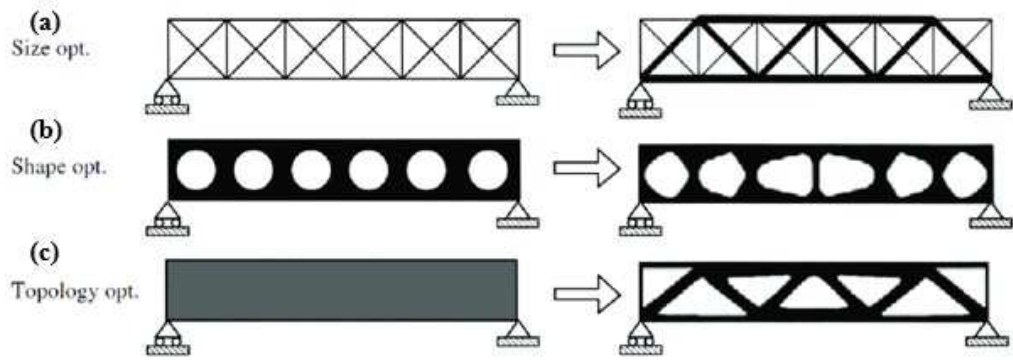


Figure 3.1: Examples for (a) Sizing optimization, (b) Shape optimization, (c) Topology optimization [34]

##### 3.1.1 Sizing Optimization

In sizing optimization, design variable is thickness distribution of design or cross sectional areas of structural members. Without changing its shape, the part is modified by changing the size of its members. For example, thickness can be a design variable for a sheet metal part corresponding to a displacement constraint.

Topometry optimization can be considered as a generalization of sizing optimization. In topometry optimization, each element is used as a design variable and sized inde-

pendently [35].

### **3.1.2 Shape Optimization**

In shape optimization, interested geometric feature is shape or contour of the structural geometry. For optimal design, the connectivity of the structure is not changed, i.e., new boundaries are not created. Instead, predetermined boundaries are changed. For example, holes are not removed from the geometry, but shape of it may be modified.

Topography optimization is a case of shape optimization. As a design variable, each element's location is used and shape of each element is determined independently [36].

### **3.1.3 Topology Optimization**

For topology optimization, number, location and shape of features, such as holes, are changed to achieve optimal design. In a design space, all elements are design variables. Optimal material distribution is determined by changing density of each design elements under specified load cases and constraints.

In this study, topology optimization method is used with a commercial product; Altair Hyperworks.

## **3.2 Method of Topology Optimization**

As mentioned, topology optimization is a structural optimization method to maximize system performance in a design volume for a given load and boundary conditions with constraints. By finding the best distribution of the material, topology optimization gives chance to gain lightweight structural parts to manufacture.

For topology optimization, design problem is defined with design volume, boundary conditions, load cases and constraints at first. In other words, the optimization problem consists of a design space with an objective function and constraints. Design space means the volume that can be reduced through optimization. Design space



changes according to the density of material in each location, in other words material distribution is used as design variable. Non-design space that is defined through problem but not modified through optimization. Objective function represents the quantity that is optimized for system performance. In general, the objective function is stiffness to maximize. Lastly, constraint function, that design should satisfy, must be defined such as maximum stress constraint. It is possible to define multiple constraints on structural problem.

By using finite element methods, the solution is reached with decreasing volume. This is done by using material density of each element. Every material density has a value on solution 0 or 1. 0 represents the void and 1 refers the presence of material. Since topology optimization directly depends on elements, large amount of elements is recommended to assign more element density and increase topological complexity. In topology optimization methods, predefined design configurations do not exist unlike shape or sizing optimization. Since the part can attain any complex shape by topology optimization in a design volume, it is generally hard to manufacture by traditional methods directly. Although machine constraints are possible to define through optimization, corrections are still needed after optimization. On the other hand, it is generally possible to manufacture optimized part by AM techniques without significant changes on design.

### **3.3 Finite Element Method**

Finite Element Method (FEM) is a numerical method to solve engineering problems such as structural analysis or heat transfer. In general, this method is seeking for an analytical solution to boundary value problems. It is performed by dividing the design space into small units named finite elements that are formed by nodes. A node is a point, located on the finite element, where the calculation of the field variable value is done. To define entire problem, finite elements are modeled by simple equations and then get together into a larger equation system.

Practical application of the FEM is called as Finite Element Analysis (FEA) which is a computational tool for engineering problems' analysis. FEA provides to solve complex problems. To divide the problem into smaller elements, mesh generation

methods are used with the help of a software that contains FEM algorithm.

### **3.4 Software Usage for Topology Optimization**

There are lots of commercial products for FEM analysis and structural optimization. Hyperworks, invented by Altair Company, is one of those products and contains sub-tools for analysis, optimization and simulation. In this study, Hyperworks' sub-tool Optistruct was used for topology optimization of an aircraft fitting.

#### **3.4.1 Optistruct**

OptiStruct is a structural optimization solver which does not have graphical interface and works with Hypermesh for problem formulation.

The solver gives chance to user to make different types of finite element analysis such as static, buckling and displacement analysis under static and dynamic loads such as pressure, gravity, point force, etc. It is also possible to make thermal, acoustic and fatigue analysis via Optistruct.

In addition to analysis, topology, topography, size and shape optimization can be performed via this solver. By using Hyperview, analysis and optimization results can be simulated.

#### **3.4.2 Topology Optimization with Optistruct**

The aim of the topology optimization is to generate an optimized material distribution for a design under specified loads and constraints. For a topology optimization, design space, constraints, load cases and also machine constraints can be defined, and optimized solution can be obtained by density method with Optistruct.

Manufacturing constraints are very important for gaining feasible models to produce after optimization. Symmetry, Min/Max member size, draw direction, extrusion constraints, etc. can be defined for optimization problem on this solver. It is also possible to create smooth surfaces and generate geometry for 3D results.

For the solution, an iterative procedure is followed by Optistruct. Analysis is per-

formed firstly by using FEM model. Secondly, convergence test is performed, response screening is done for current iteration. Design sensitivity analysis is made and optimization of the problem is formulated by using sensitivity results and go back to first step for each iteration until the gain feasible design. Optistruct solver is using density method to solve topology optimization problems. In this method, each finite element takes a value of 0 or 1 to be define the element is either void or solid.

User should define design, non-design spaces, material properties, load cases, optimization parameters (such as draw direction) and responses for objective and constraint functions. Mass, volume, static displacement, natural frequency, and compliance are some of the responses that can be defined on the solver. Definition of the main terminologies for optimization are as follows:

Design Space: The space that material removal is applied according to optimization constraints, i.e. designable part of the problem.

Non-Design Space: The space that remains constant after optimization.

Design Variable: Parameters to optimize system performance. For a topology optimization with density method, the material density of each element is used as design variable. It can be defined for solid, Shell or 1D elements with machine constraints.

Constraint function: For a feasible design, bounds on defined response of the problem. A range for mass fraction can be an example for constraint function.

Objective function: The function of the response to be optimized. The function can be minimized, maximized or reached a given value of related response. For example: minimizing compliance.



## **CHAPTER 4**

### **EXPERIMENTAL STUDY**

This part of the thesis contains the producing samples and related tests to understand mechanical properties of Ti6Al4V parts produced by EBM.

#### **4.1 Experimental Procedure**

Nine samples with three different building directions were produced by ARCAM Q20 EBM Machine. Throughout the process, same parameters were used except building direction. Supporting geometries were removed by grinding and one of the samples on each direction was machined by lathe to see effects of surface imperfections on mechanical properties. After manufacturing of the samples, tensile tests were performed to get mechanical properties. Surface roughness and fracture surfaces were also examined.

#### **4.2 Manufacturing of the Samples**

##### **4.2.1 Properties of the Samples**

Samples were produced with ARCAM Ti6Al4V powder according to ASTM E8M Standard with the dimensions shown in Figure 4.1. 1mm excess in diameter was given to exact geometry for the manufacturing process due to expected surface imperfections. Chemical Properties of the powder can be seen in Table 4.1. Particle size of the ARCAM Ti6Al4V powder is between 45 and 100  $\mu\text{m}$ .

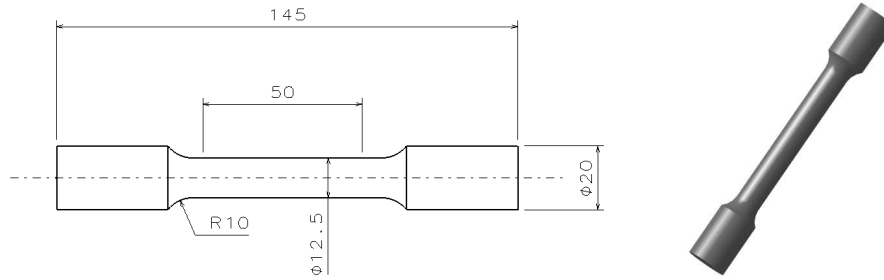


Figure 4.1: Dimensions of the tensile test specimen according to ASTM E8M (Dimensions are in mm)

Table 4.1: Chemical composition of the ARCAM Ti6Al4V powder [37]

Aluminum, Al	6%
Vanadium, V	4%
Carbon, C	0.03%
Iron, Fe	0.10%
Oxygen, O	0.15%
Nitrogen, N	0.01%
Hydrogen, H	0.00%
Titanium, Ti	Balance

#### 4.2.2 Process Parameters

All of the specimens were built by the same process parameters supplied and recommended by the company as shown in Tables 4.3 to 4.4.

Only building direction was different for the specimens. Building direction and location of the specimens in chamber are shown in Figure 4.2. WCS means work coordinate system and X, Y and Z are the building directions.

#### Scanning Strategy

The algorithm identified by ARCAM Company was used as scanning strategy. EBM Control Software optimizes combination of lines, angle and virtual movement of hatches to reach more homogeneous metallurgy without operator dependence.

In EBM building procedure, preheating process consists of two stages. While preheat-1 scans the entire bed, preheat-2 pre-scans the islands to be melted which are defined by the algorithm according to the location, shape and size of the part to be built. Then,

Table 4.2: Process parameters for preheat operation

<b>Preheat</b>	Focus Offset	44 mA	
	Heating Focus Offset	100 mA	
	Maximum Heat Time	60 s	
	Square Size	144 mm	
	Offset to Part	4 mm	
	Max. Current	48 mA	
	Preheat I	Max. Beam Current	36 mA
		Min. Beam Current	36 mA
		Beam Speed	40500 mm/s
		Number of Repetitions	3
		Line Offset	0.4 mm
		Hatch Depth	0.09 mm
	Preheat II	Max. Beam Current	45 mA
		Min. Beam Current	45 mA
		Beam Speed	40500 mm/s
		Number of Repetitions	3
		Line Offset	0.4 mm
		Hatch Depth	0.09 mm

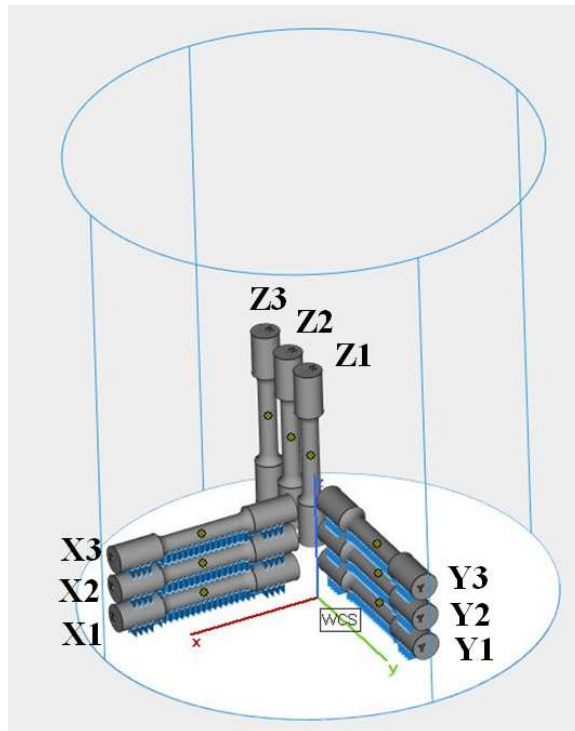


Figure 4.2: Building directions of the specimens and their locations in vacuum chamber according to machine coordinate system

Table 4.3: Process parameters for melt operation

<b>Melt</b>	Surface Temperature	925 °C		
	Max. Depth for Curr. Add	65 mm		
	Contours	Number of Contours	3	
		Outer Contours	Beam Speed	500 mm/s
			Max. Beam Current	9 mA
			Beam Offset	0.27 mm
			Multispot Speed	80000 mm/s
		Inner Contours	Beam Speed	550 mm/s
			Max. Beam Current	9 mA
			Beam Offset	0.18 mm
			Multispot Speed	80000 mm/s
	Hatch	Max. Beam Current	28 mA	
		Line Offset	0.22 mm	
		Hatch Depth	0.09 mm	
		Min. Current	3.5 mA	
		Scan Length Ref	45 mm	

Table 4.4: Process parameters for wafer operation

<b>Wafer</b>	Repetitions	2
	Min. Distance of Repetitions	0.9 mm
	Multispot Speed	140000 mm/s
	Current	10 mA
	Speed	1950 mm/s
	Focus Offset	9 mA



Table 4.5: Process parameters for net operation

Net	Surface Temperature	750 °C		
	Max. Depth for Curr. Add	5000 mm		
	Contours	Number of Contours	4	
		Outer Contours	Beam Speed	400 mm/s
			Max. Beam Current	3.2 mA
			Beam Offset	0.2 mm
			Multispot Speed	10000 mm/s
		Inner Contours	Beam Speed	400 mm/s
			Max. Beam Current	3.2 mA
			Beam Offset	0.08 mm
			Multispot Speed	10000 mm/s
	Hatch	Max. Beam Current	3 mA	
		Line Offset	0.2 mm	
		Hatch Depth	0.07 mm	
		Min Current	0 mA	
		Scan Length Ref	70 mm	

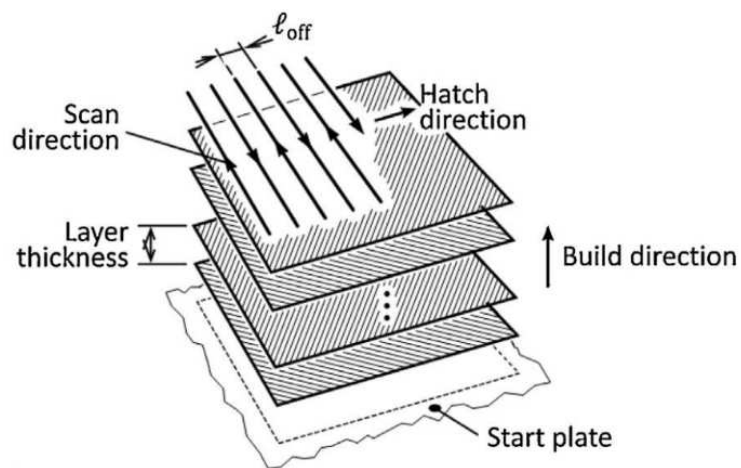


Figure 4.3: An example for layer by layer building process [38]

building sequence continues with melting process [39].

Melting stage starts with contours that formed the outside of each island. Multi Beam Technology is used for forming of contours to keep several melt pools active at the same time. According to the defined algorithm, outer contour is formed slowly with lower power than the inner contours. After forming contours, islands are filled with hatches with a continuous path [39]. An example for scanning strategy used by EBM can be seen in Figure 2.7.

EBM Control Software adjusts the beam current according to length of each hatch line (i.e. scan length), and changes the hatch angle between each layer. An example for the layer by layer building of an island can be seen in Figure 4.3.

#### 4.2.3 Samples Built by EBM

Visuals of X, Y, Z samples after manufacturing are shown in Figures 4.4 and 4.5. There are no support geometries for samples built in Z direction, i.e. vertical specimen. But for X and Y samples, auxiliary geometries exist since they were manufactured on top of each other horizontally.

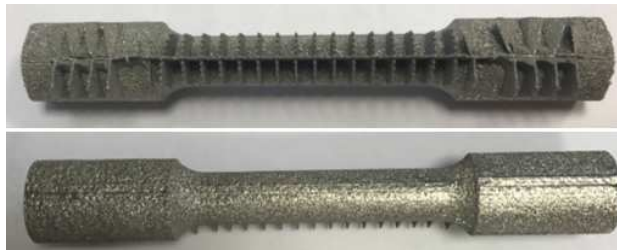


Figure 4.4: Side views of X and Y specimens with support geometries after manufacturing by EBM



Figure 4.5: As-built Z specimen

#### 4.2.4 Post Process

For the X and Y specimens, support geometries were cleaned up by grinding as shown in Figure 4.6. To see the effect of surface imperfections on mechanical properties, one of the samples in each direction was machined by lathe 1mm in diameter to the exact geometry.



Figure 4.6: A sample of X and Y specimens after grinding operation



Figure 4.7: Visual of a post machined specimen

In Edwards et al.'s study, manufacturing process was done at the elevated temperature in the build chamber to decrease residual stress during solidification and cooling of the melted layers. And they have not performed stress relief post process. But they indicated that if the concern is porosity or fatigue life instead of tensile properties, stress relief heat treatment was required [4].

In addition to surface roughness, Formanoir et al. have also examined heat treatment after manufacturing and they showed that it does not have huge effect on tensile prop-

erties [10].

Since the main concern of this study is tensile properties of EBM parts, stress relief heat treatments were not applied.

### 4.3 Tensile Test

Tensile test procedure was conducted according to standard test method ASTM E8-11 for tension testing of metallic materials. The tests have been carried out at 25°C and 50% humidity rate. INSTRON Static Axial Clip-on extensometer with gauge length 25mm has been used to measure of the specimens' true strain and extension rate. Tensile test setup was installed as shown in Figure 4.8.



Figure 4.8: Tensile test setup

#### 4.3.1 Mechanical Properties of the Samples Built by EBM

Test results were taken via a computer system connected to setup. The graphical results for each specimen can be seen from Figure 4.9 to Figure 4.26,

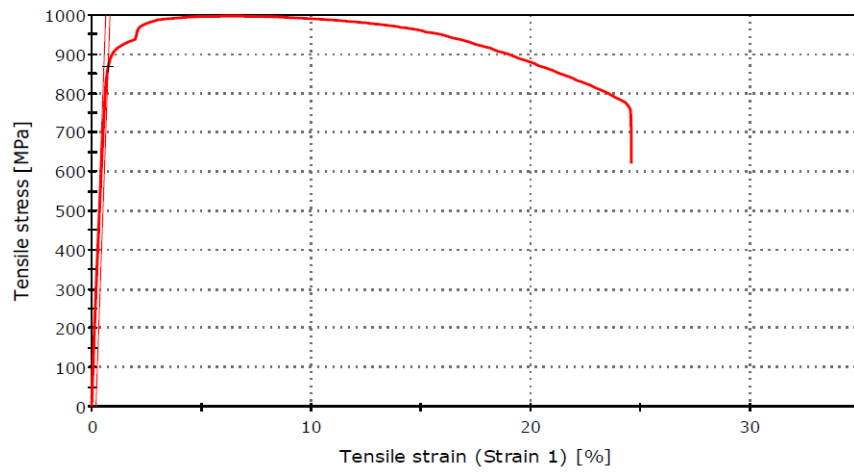


Figure 4.9: X1 tensile stress vs. tensile strain graph

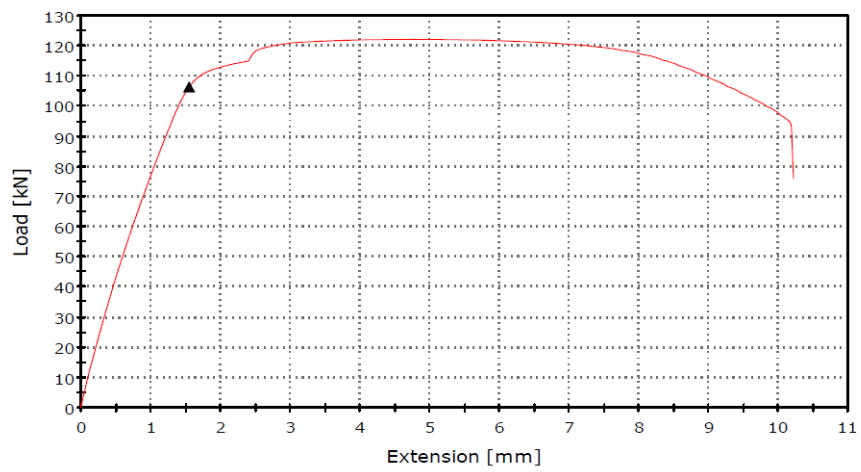


Figure 4.10: X1 extension vs. load graph

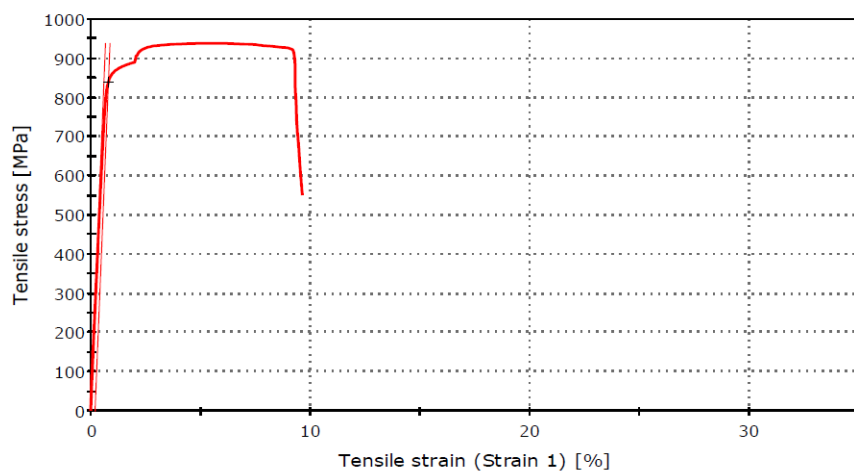


Figure 4.11: X2 tensile stress vs. tensile strain graph

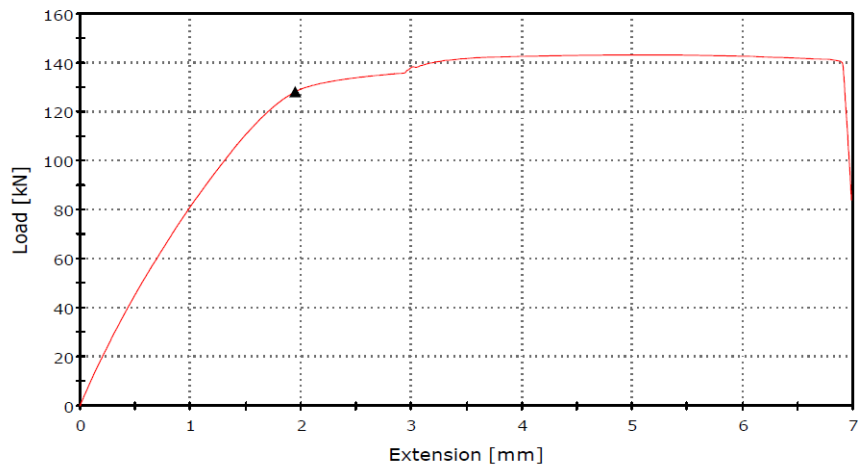


Figure 4.12: X2 extension vs. load graph

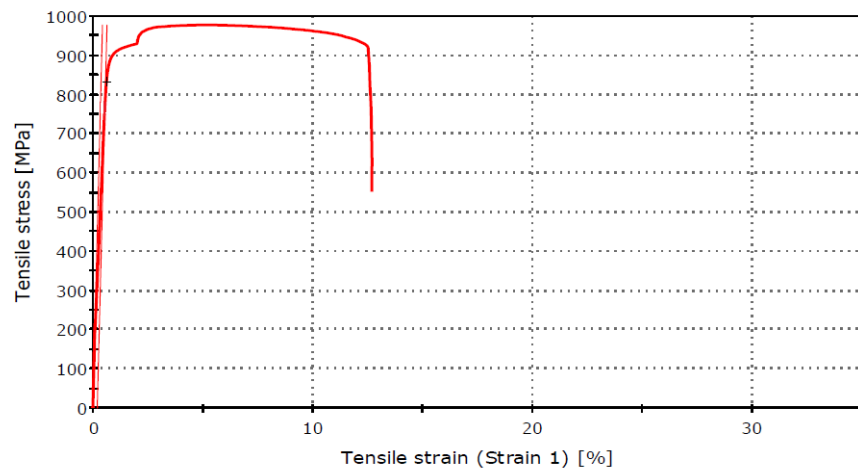


Figure 4.13: X3 tensile stress vs. tensile strain graph

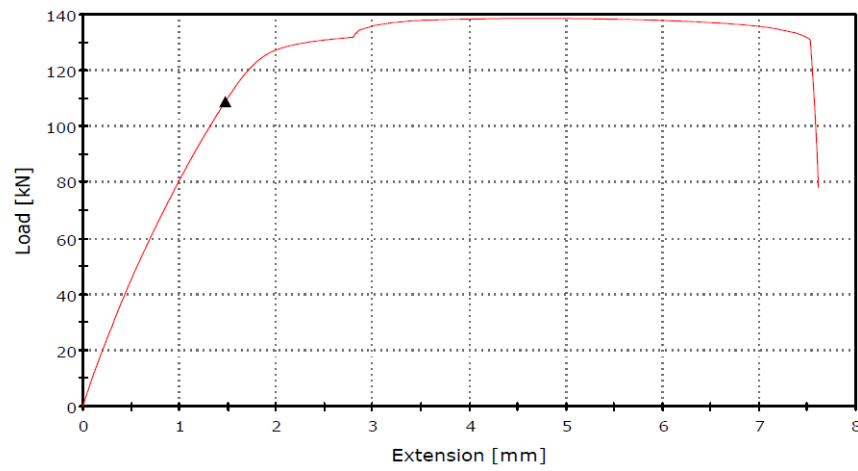


Figure 4.14: X3 extension vs. load graph

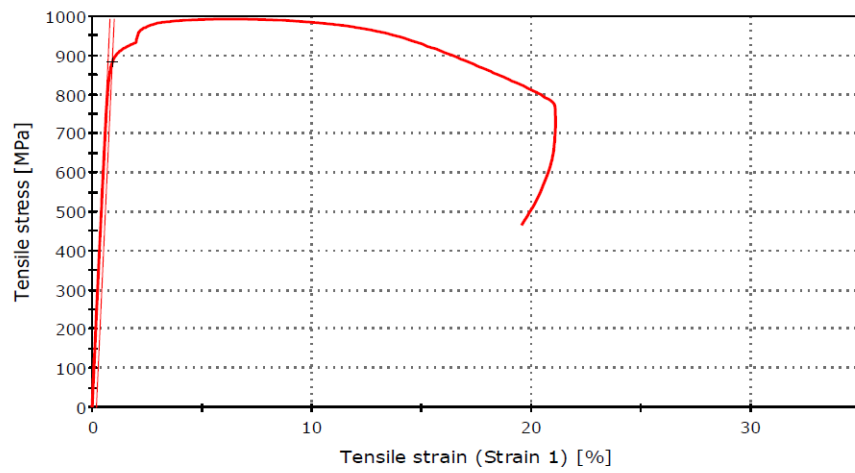


Figure 4.15: Y1 tensile stress vs. tensile strain graph

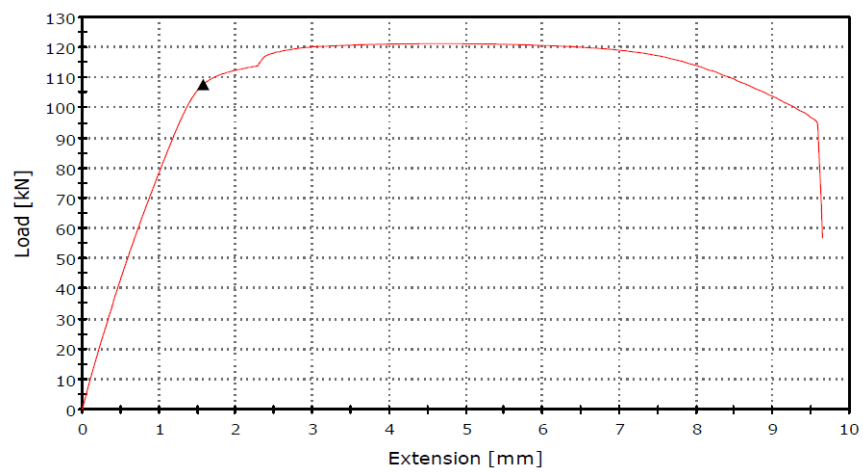


Figure 4.16: Y1 extension vs. load graph

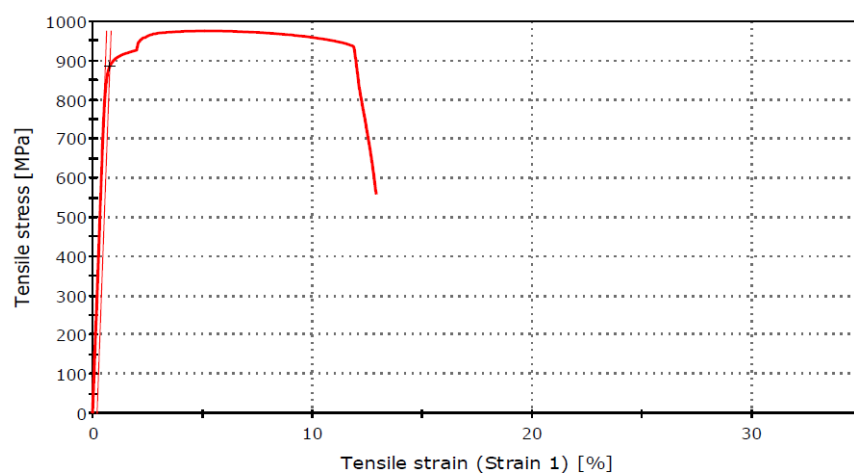


Figure 4.17: Y2 tensile stress vs. tensile strain graph

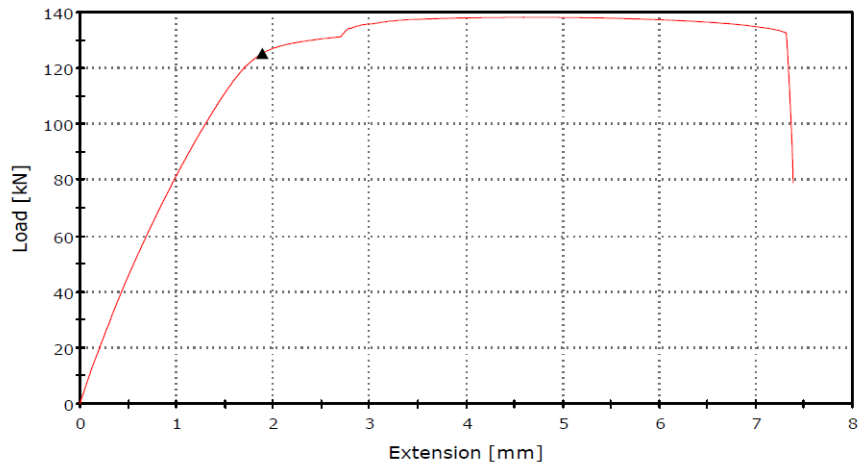


Figure 4.18: Y2 extension vs. load graph

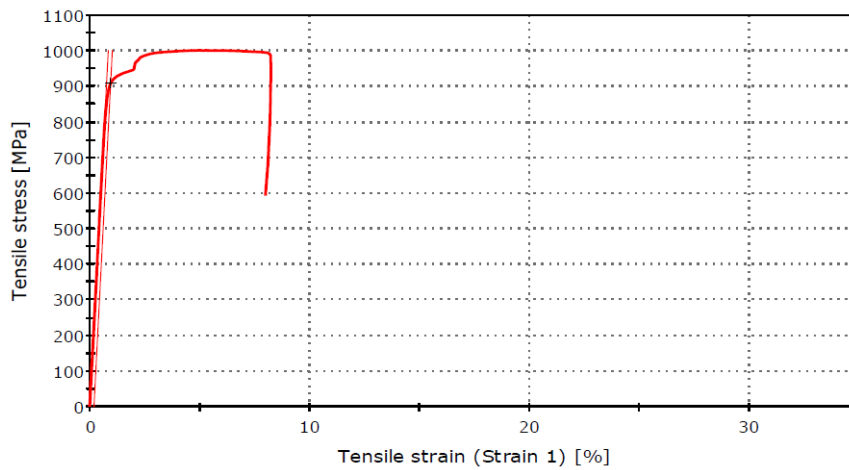


Figure 4.19: Y3 tensile stress vs. tensile strain graph

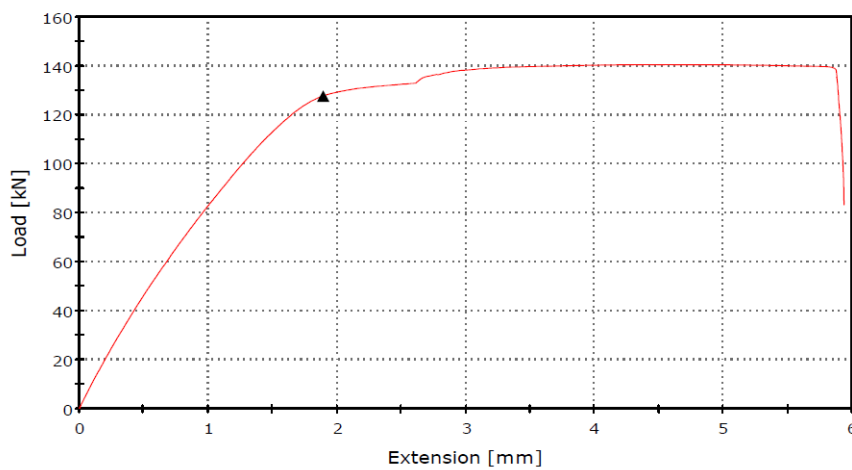


Figure 4.20: Y3 extension vs. load graph



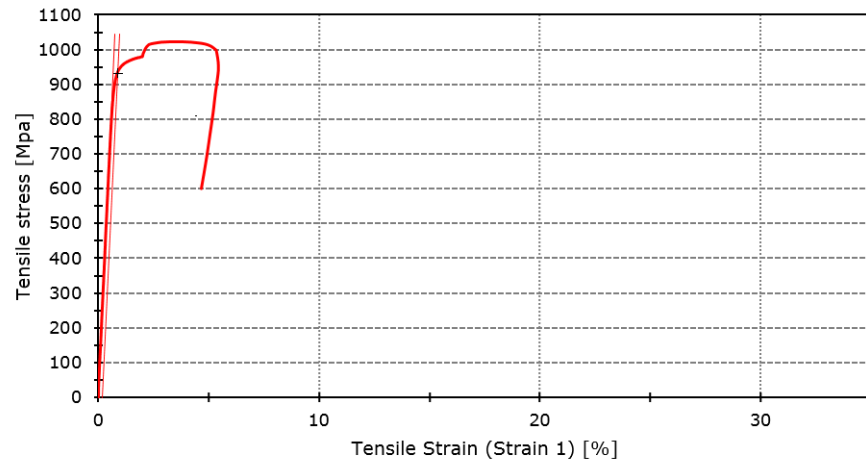


Figure 4.21: Z1 tensile stress vs. tensile strain graph

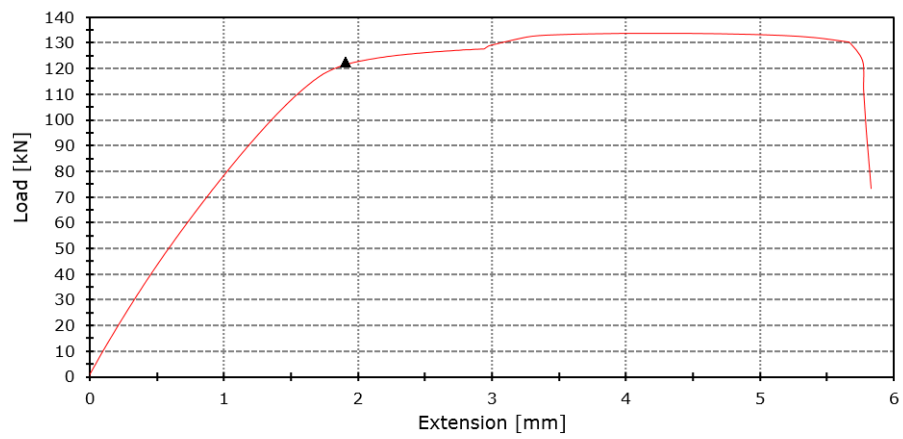


Figure 4.22: Z1 extension vs. load graph

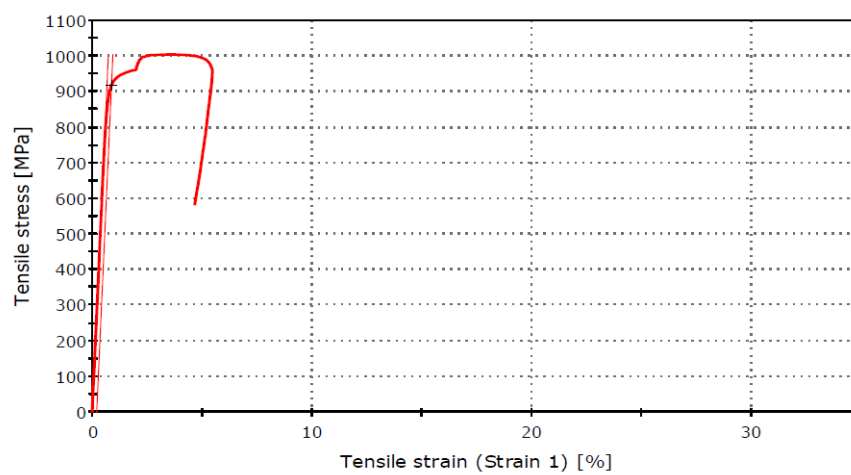


Figure 4.23: Z2 tensile stress vs. tensile strain graph

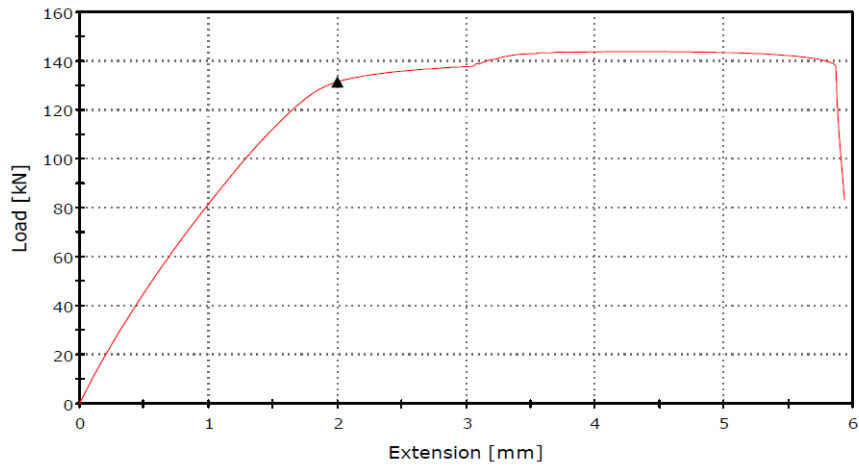


Figure 4.24: Z2 extension vs. load graph

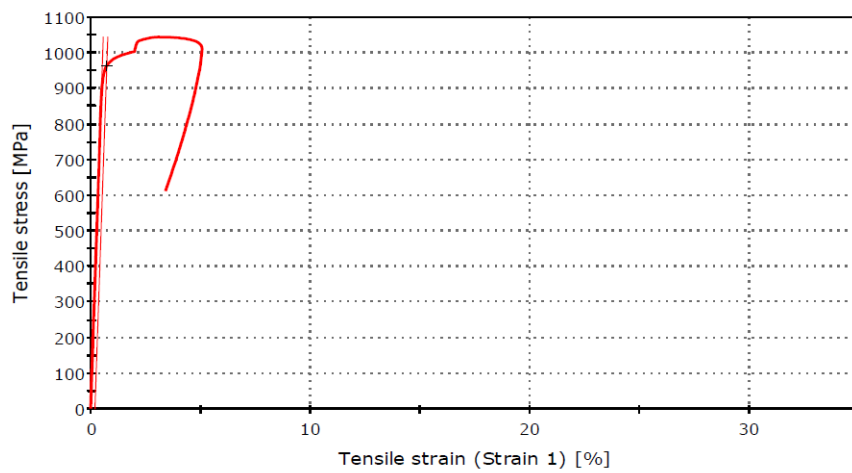


Figure 4.25: Z3 tensile stress vs. tensile strain graph

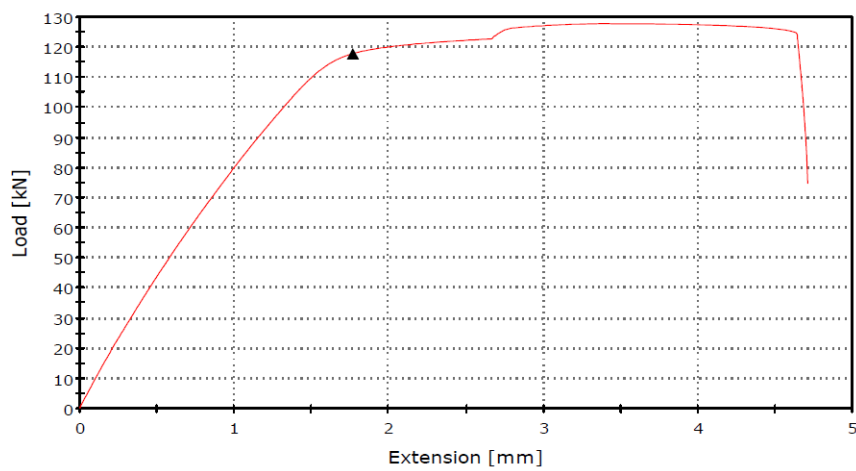


Figure 4.26: Z3 extension vs. load graph

UTS, YS and E values were taken for each specimen from the results graphs. Percentage of elongation for each one is also found from extension versus load graphs by dividing extension at fracture to initial length. All related values from the test were represented at Table 4.6.

Table 4.6: Tensile properties of the specimens

Specimen Name	Diameter [mm]	Ultimate Tensile Strength [Mpa]	Yield Strength (Offset 0.2%) [MPa]	Young's Modulus [GPa]	Elongation [%]
X1 (Machined)	12.49	999.6	868.1	156.9	24
X2 (As-built)	13.54	938	839.5	138.2	14
X3 (As-built)	13.44	976.6	836.7	172.3	15
Y1 (Machined)	12.47	992.4	881.7	122	19
Y2 (As-built)	13.43	975.3	884.6	153.8	15
Y3 (As-built)	13.37	1000.5	909.2	118.9	12
Z1 (Machined)	12.48	1023.7	942.1	152.7	12
Z2 (As-built)	13.51	1003.4	917	136.6	12
Z3 (As-built)	13.49	1044.2	963.3	180	9

Average values and standard deviations are compared according to building direction on Table 4.7.

Table 4.7: Comparison of the results by building direction

	X Samples	Y Samples	Z Samples
<b>Ultimate Tensile Strength [MPa]</b>	967±29	988±13	1023±21
<b>Yield Strength (Offset 0.2%) [MPa]</b>	852±16	895±14	940±23
<b>Young's Modulus [GPa]</b>	155±17	136±17	158±22
<b>Elongation [%]</b>	19±5	15±4	10±2

The average value of the tensile properties for the Y specimens is better than the X specimens as seen in Table 4.7. However, while examining each specimen separately, it can be seen from Table 4.6 that there are X specimens have better results than Y specimens while Z specimens are always better than X and Y specimens. Since they were built in the same direction according to the applied load for the tensile test, the difference between the X and Y specimens might occur because of the scanning strategy that defined as an algorithm . Related studies show that scanning strategy has an important role in final properties of the parts [40, 41].

Therefore, as compatible with the literature [4, 9, 10], while examining the effect of building direction, evaluating the X and Y specimens together as horizontal parts can be more suitable, since scanning strategy, hatch angle and length are defined by EBM control software as mentioned in Section 4.2.2.

The results show that Z samples have higher UTS, YS and E values than X and Y samples. Z specimens have also lower elongation rates than X and Y specimens. While comparing machined and as-built parts, it can be seen from the Table 4.6, machining of the rough surfaces has not a direct effect on mechanical properties. In their study, Edwards et al. state that machining of the surface is more critical for fatigue characteristics than tensile properties [19].

In Al-Bermani et al.'s research on mechanical properties of Ti6Al4V parts produced by EBM, the similar results have been obtained with our study. They found that UTS is between 993.9 and 1031.9 MPa, YS between 883.7 and 938.5 MPa, and % elongation between 11.6 and 13.6 [14].

In their study, Zhai et al. had similar results while examining EBM building direction effects and concluded that building direction changed from X or Y to Z direction, i.e. horizontal to vertical direction, tensile direction also changed and UTS and YS increased [9]. Test results from another study by Hrabe and Quinn also showed that the elongation is higher in the X and Y directions compared to Z direction [3].

#### **4.3.2 Comparison of the Results with Cast and Wrought Material Properties**

Comparison of the test results of EBM parts with cast and wrought parts are given in Tables 4.8 and 4.9.

Table 4.6 with Table 4.9 show that overall values of test results are better than cast and wrought material properties while the values of samples built in Z direction are closer to the values supplied by the machine company than those built in X and Y. Some other studies also show that the mechanical properties of Ti6Al4V parts produced by EBM have better tensile properties than cast and wrought ones. Hrabe and Quinn's research, for example, results with a value of 1009-1033Mpa for UTS and 961-984Mpa for YS which are comparable with company values [3]. In another study from Zhai et al., YS was found between 973-1051MPa and UTS was found between 1032-1116MPa for Ti6Al4V specimens manufactured by EBM in different building

Table 4.8: Comparison of chemical properties of the ARCAM Ti6Al4V powder to cast and wrought Ti6Al4V materials

	<b>ARCAM Ti6Al4V Powder*</b>	<b>Cast Ti6Al4V Material**</b>	<b>Wrought Ti6Al4V Material***</b>
<b>Aluminum, Al</b>	6%	5.5–6.75%	5.5–6.75%
<b>Vanadium, V</b>	4%	3.5–4.5%	3.5–4.5%
<b>Carbon, C</b>	0.03%	<0.1%	<0.8%
<b>Iron, Fe</b>	0.10%	<0.3%	<0.3%
<b>Oxygen, O</b>	0.15%	<0.2%	<0.2%
<b>Nitrogen, N</b>	0.01%	<0.05%	<0.05%
<b>Hydrogen, H</b>	0.00%	<0.015%	<0.015%
<b>Titanium, Ti</b>	Balance	Balance	Balance

\*Given by ARCAM Company

\*\*Required values according to ASTM F1108

\*\*\*Required values according to ASTM F1472

Table 4.9: Comparison of mechanical properties of the tensile specimens with ARCAM Ti6Al4V powder, cast and wrought Ti6Al4V materials

	<b>Tensile Test Results (Overall)</b>	<b>ARCAM Ti6Al4V Powder*</b>	<b>Cast Ti6Al4V Material**</b>	<b>Wrought Ti6Al4V Material***</b>
<b>Ultimate Tensile Strength [MPa]</b>	995	1020	860	930
<b>Yield Strength (Offset 0.2%) [MPa]</b>	894	950	758	860
<b>Young's Modulus [GPa]</b>	148	120	114	114
<b>Elongation [%]</b>	15	14	>8	>10

\*Given by ARCAM Company

\*\*Required values according to ASTM F1108

\*\*\*Required values according to ASTM F1472

directions [9].

In their study, Formair et al. reported that tensile properties in different papers are changing in a very large range [10]. These differences may have occurred because of post processing or dissimilar process parameters. Gong et al., for example, tested EBM parts produced with different process parameters in their research and they had significantly different results for each case [13]. That shows the importance of testing parts in the same condition.

#### 4.4 Surface Roughness Tests for Samples

For roughness measurements, Mahr MarSurfM300 model surface roughness tester shown in Figure 4.27 was used. For each specimen, measurements were taken from five different locations on specimen through its length linearly and the average values were used for  $R_a$  and  $R_z$ .  $R_a$ , is the arithmetical mean roughness value of the surface deviations from the roughness profile mean line. And  $R_z$  is the average of the five greatest height of roughness profile.



Figure 4.27: Mahr model surface tester

Table 4.10 shows  $R_a$  and  $R_z$  measurements of the specimens. As shown in the Table 4.10, machined specimens have improved surface roughness as expected. While examining Table 4.6, machined X and Y specimens have higher elongation rates and those results agreed with Formanoir's research that investigated the surface finish operations effects on mechanical properties and stated that elongation rates increase

Table 4.10:  $R_a$  and  $R_z$  values of the tensile specimens

Specimen Name	$R_a$ [ $\mu m$ ]	$R_z$ [ $\mu m$ ]
<b>X1 (Machined)</b>	0.99	5.44
<b>X2 (As-built)</b>	17.68	79.51
<b>X3 (As-built)</b>	10.58	54.84
<b>Y1 (Machined)</b>	0.77	4.52
<b>Y2 (As-built)</b>	8.56	45.57
<b>Y3 (As-built)</b>	16.99	83.31
<b>Z1 (Machined)</b>	0.62	3.57
<b>Z2 (As-built)</b>	18.2	87.89
<b>Z3 (As-built)</b>	14.8	74.88

with improving surface finish [10].

For the specimens built in Z direction, similar roughness was observed all around the circumference. For X and Y specimens, it was expected to observe difference in roughness values between top-side and down side faces because of the difference between over-melt zones. However, measurements were only taken from the sides without support geometry for those parts and it is hard to generalize all geometry with those values and to compare with Z samples. Surfaces cleaned by grinding were not included in the roughness measurement but they probably affected the elongation rates for X and Y specimens.



Figure 4.28: ZEISS Sigma 300 Scanning Electron Microscope

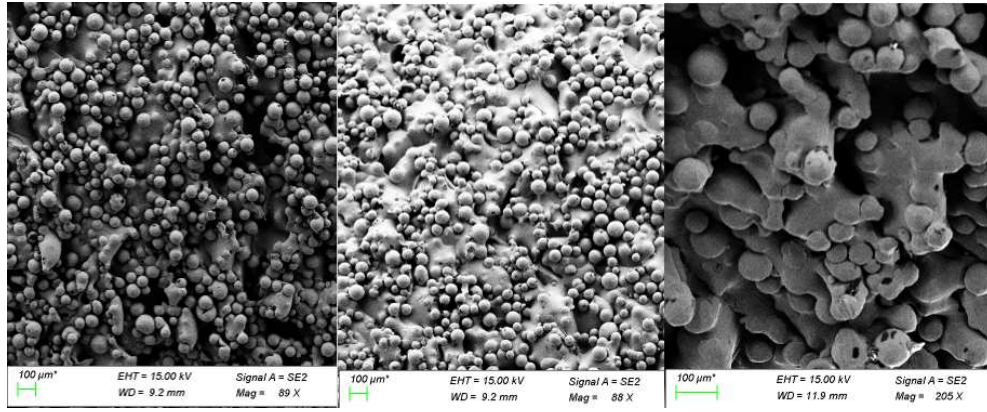


Figure 4.29: SEM pictures from the surfaces of as-built Z samples

Higher surface roughness values were observed for all as-built parts. Some SEM pictures of surfaces of the as-built Z samples were taken by ZEISS Sigma 300 Scanning Electron Microscope (SEM) (shown in Figure 4.28) and were represented in Figure 4.29. The pictures were captured from the outer surface of the specimens through their length. There are significant number of non- melted powders and porosities. Some powders cannot be fully melted, stuck to the melt pool and cause the surface irregularity. Porosities may have been observed because of the powder production process and bad melting at the sides [42].

#### 4.5 Fracture Surface Analysis



Figure 4.30: Stereo Zoom Microscope setup



After tensile test, fracture surface images of one of the specimens built in each direction were taken by Nikon SMZ-U Stereo Zoom Microscope shown in Figure 4.30. Figure 4.31 shows the images of the fracture surfaces of the specimens and Figure 4.32 illustrates the image of specimens after tensile test for machined and as-built parts.

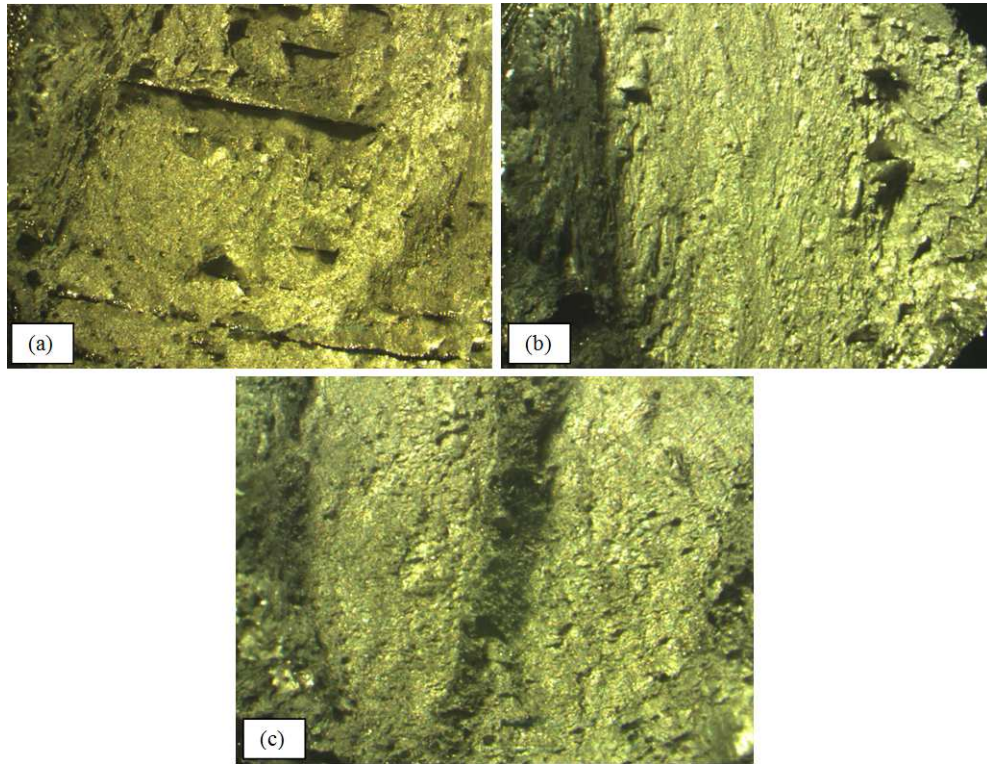


Figure 4.31: Fracture surfaces of specimens (a) X2, (b) Y2 and (c) Z2

As seen in Figure 4.32, machining parts results with a typical necking while as-built parts displayed shear fracture with lower necking due to surface roughness. While comparing with the study of Schulze et al., they had the similar results, cup and cone fractures. Only one of the specimens revealed a shear fracture in lower necking in their study [43].

In their research, Shunmugavela et al. compared the microstructure and mechanical properties of wrought and AM Ti6Al4V. By using SEM, they examined the fracture surfaces and showed that AM parts displayed small size shallow dimples that indicated brittle characteristics while surface profile of wrought one displayed deep dimples that indicated the ductile behavior of the material [44].

Quenard et al. have also examined tensile fracture surfaces of additively manufac-

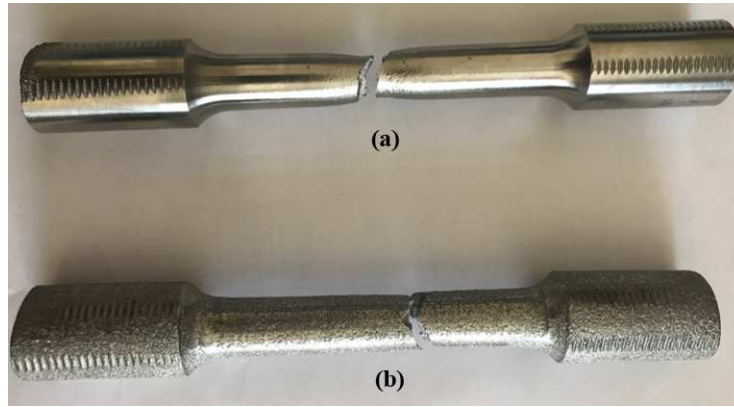


Figure 4.32: Visuals of (a) machined X specimen (b) one of the as-built Z specimens after tensile test

tured Ti6Al4V, and showed that the failure mechanism was mostly ductile. They also observed the micro cracks with brittle surfaces around them. They attributed those brittle surfaces to cleavage within layers joining two ductile surfaces and concluded that although a mixed ductile-brittle behavior was displayed, the ductility of the samples was dominating [45].

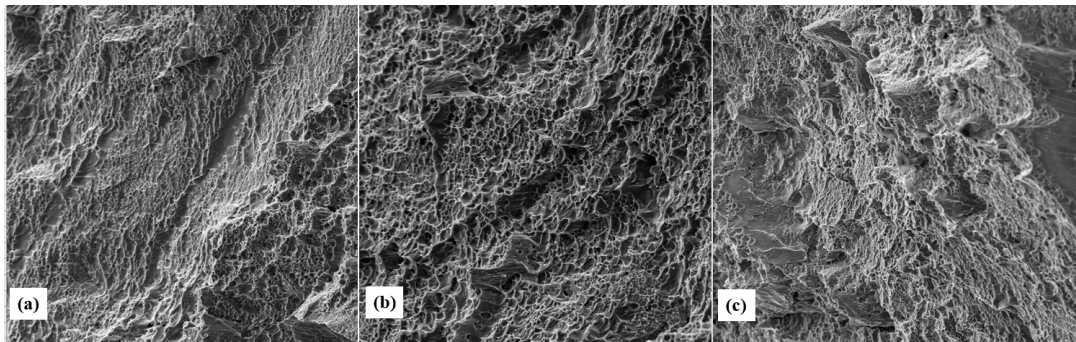


Figure 4.33: SEM pictures of the fracture surfaces of (a) X2, (b) Y2 and (c) Z2

As compatible with the literature, specimens displayed a mixed ductile-brittle fracture characteristic as seen in Figure 4.33 that represents the one of the as-built parts in each direction. Mostly deep dimples were displayed but there were still brittle surfaces between those dimples. In Z samples, more brittle surfaces were observed than other specimens.

While examining the fracture surface of machined X sample, that have the highest elongation rate, brittle surfaces rates were very low compared to ductile ones. (See Figure 4.34). Therefore, SEM analysis suits with the results of tensile test and elon-

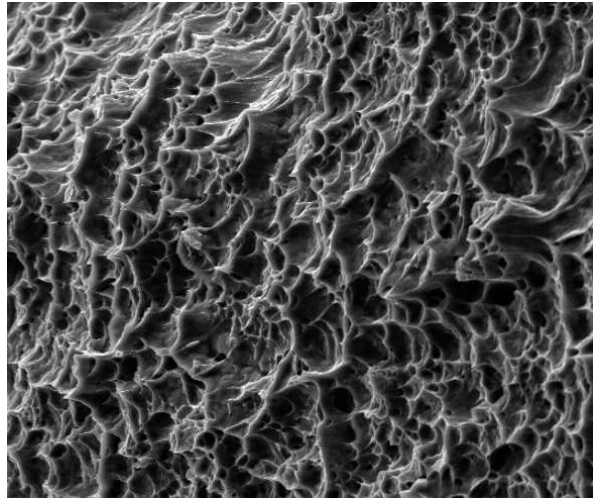


Figure 4.34: SEM picture of the fracture surface of machined X specimen

gation rates of the samples and the fact that amount of the brittle modes affect the ductility of the specimens and have a significant effect on elongation rates.

#### 4.6 Microstructure

Mechanical properties for EBM Ti6Al4V widely vary between sources. Similar studies showed conflicting results. Those differences between the related researches may be attributed to the different process parameters that cause different microstructure and mechanical properties. Building direction, is one of these process parameters, has a direct effect on final properties due to anisotropic microstructure of parts produced by EBM [46].

To examine the microstructure, the specimens were cut from their circular cross section. After that, the specimens were mounted in bakelite by using black phenolic powder at Metkon Ecopress 50 Mounting Press (See Figure 4.35). Specimens with 40mm diameter were obtained by melting powders at 190°C for three minutes.

After bakelite mounting process, the grinding operation was done with Silicon Carbide (SiC) abrasive, and the polishing was done with Aluminum Oxide (Al<sub>2</sub>O<sub>3</sub>) solution by using Buehler Beta Grinder- Polisher shown in Figure 4.36.

Finally, the etching process took place by using Kroll's Reagent etchant. And, the microstructures of the specimens were examined via Leica DM2700 M Optical Microscope shown in Figure 4.37.



Figure 4.35: Metkon Ecoperss 50 Mounting Press



Figure 4.36: Buehler Beta Grinder-Polisher





Figure 4.37: Leica DM2700 M Optical Microscope

Ti6Al4V is comprised of  $\alpha$  and  $\beta$  phases where  $\alpha$  phase has a hexagonal close packed crystal structure while  $\beta$  phase has a body centered cubic crystal structure. In this alloy, Al is used to stabilize  $\alpha$  phase at higher temperatures while V is used to stabilize  $\beta$  phase at lower temperatures. [47]

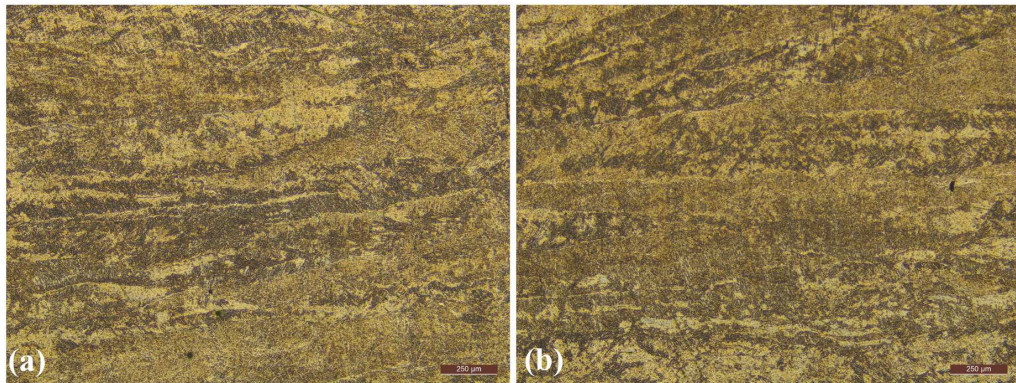


Figure 4.38: Microstructure of (a)X2 specimen, (b)Y2 Specimen

Figure 4.38 and Figure 4.39 represent the optical microscope pictures of the circular cross section of the specimens. The section of the X specimen illustrates YZ plane, and the section of the Y specimen illustrates XZ plane of the machine. Represented structures with these planes are oriented parallel to building direction (i.e. Z axis),

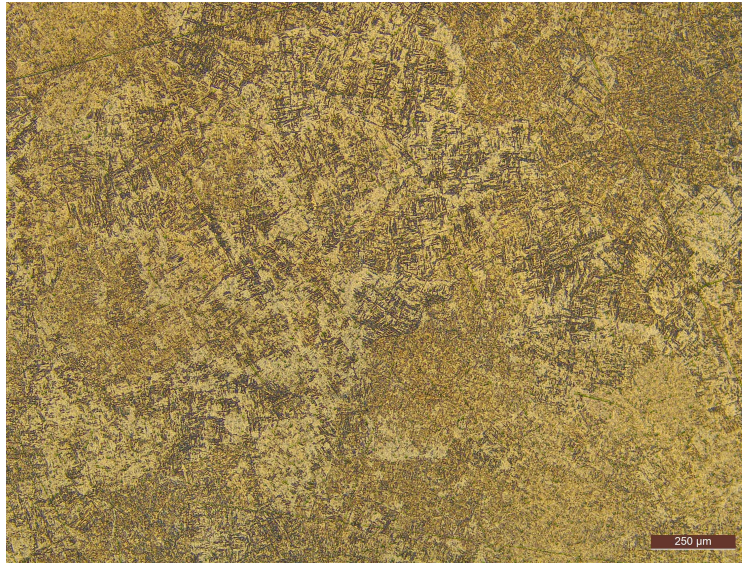


Figure 4.39: Microstructure of Z2 specimen

and a prior  $\beta$  columnar structure can be observed from the pictures. On the picture of the Z specimen, XY plane and the structure perpendicular to building direction are represented, and perpendicular sections of the columnar grains can be observed. (See Figure 4.2 for the orientation of the specimens.)

The dark phase represents the  $\beta$  phase while  $\alpha$  phase is represented with the light phase at the pictures. The microstructures of the specimens are inhomogeneous although they are fine. Basket weave and colony pattern  $\alpha+\beta$  lamellar structure in equiaxed microstructure displayed for Z specimen and it was observed that grain size varies in different locations.

At the sections of X and Y specimens, the microstructure is mainly basket weave and  $\alpha+\beta$  lamellar microstructure was observed inside the prior  $\beta$  grains, while the size of  $\alpha$  and  $\beta$  laths varied in different locations.

The microstructure with similar visuals have been described and characterized extensively in previous studies [4, 8, 9, 46, 48].

For the Z specimens, lower elongation rates were observed in our study. This may be because of the columnar grains that are parallel to the applied load through tensile test. Similar relationship may be linked between grain direction and higher tensile strength of the Z specimens. Bass had a similar conclusion in his study where the microstructure and mechanical properties of Ti6Al4V were evaluated by using optical and electron microscopy and tensile testing[49].

## CHAPTER 5

### TOPOLOGY OPTIMIZATION OF AN AIRCRAFT FITTING

In this section, a titanium aircraft fitting was optimized according to the experimental data. Firstly, main design was analyzed according to the defined loads and boundary conditions, and after that design was optimized to be manufactured by EBM. Two topology optimizations were conducted for vertical and horizontal orientations to see effect of building direction on the last design solution.

Hyperworks 2017, by Altair Engineering Company, was used for topology optimization part of the thesis. Hypermesh was used for meshing operation, load and boundary condition definitions. Optistruct was used for analysis and optimization operations. Hyperview was used to simulate the results of analysis and optimization. Lastly, Ossmooth was used to gain 3D CAD data with smooth surfaces and meshing for reanalysis of the final designs.

#### 5.1 Optimization Model

Figure 5.1 shows the part to be optimized which is one of the aircraft fitting that attaches two main components of the aircraft. The material for the part is cast Ti6Al4V. All boundary conditions, loads, limitations and shape are predefined and they are not discussed or changed in this study.

Figure 5.2 represents that how the fitting is attached to other components and the design space of the part.

As shown in Figure 5.2, parts are attached to one of the component via two bolt-nut sets, and to the other with a bushing. Design space limitations on z axis are shown in Figure 5.2-a and on y axis are shown in Figure 5.2-b.

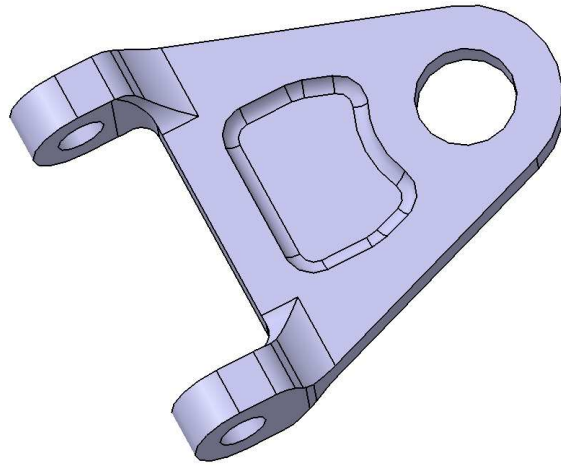


Figure 5.1: An aircraft fitting that connects two main components

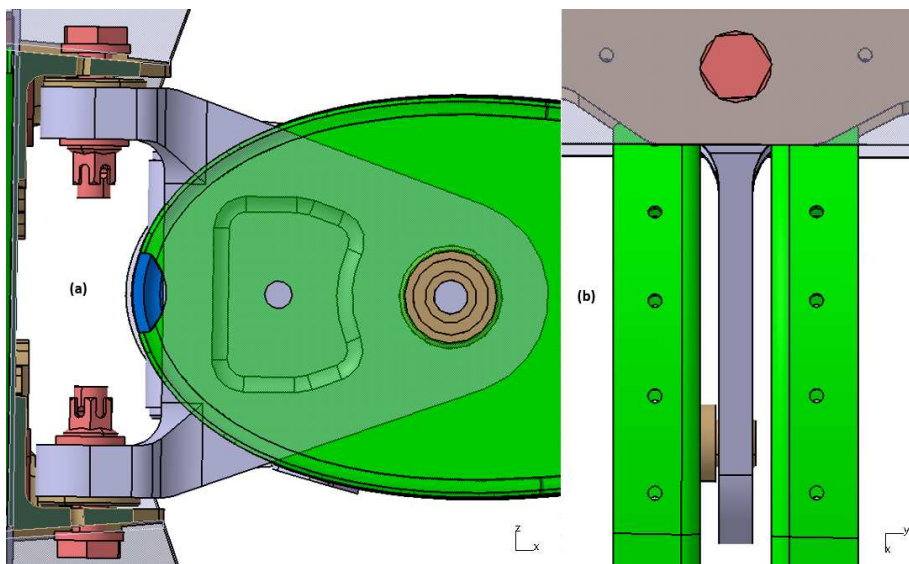


Figure 5.2: (a) Side-section view of the assembly, (b) Top view of the assembly according to aircraft coordinate system



While thinking free body diagram of the fitting, it is assumed that only the lower fastener carries the load in Z direction and both fasteners carry the load in X direction according to Figure 5.2-a. And the loads are applied on bushing connection.

### 5.1.1 Finite Element Model

FEM model was created by using Hypermesh tool. TET10 solid element type was used and order of all elements was changed to second order for accurate solution. The element size was chosen as 0.5 to be compatible with optimization model. Why 0.5 was used as element size is described in Section 5.3.5.

Bolt connections of the part were created as RBE2 element by using a calculated center node from nodes on hole for each bolt connection. RBE3 element type was used for bushing connection again with a calculated center node.

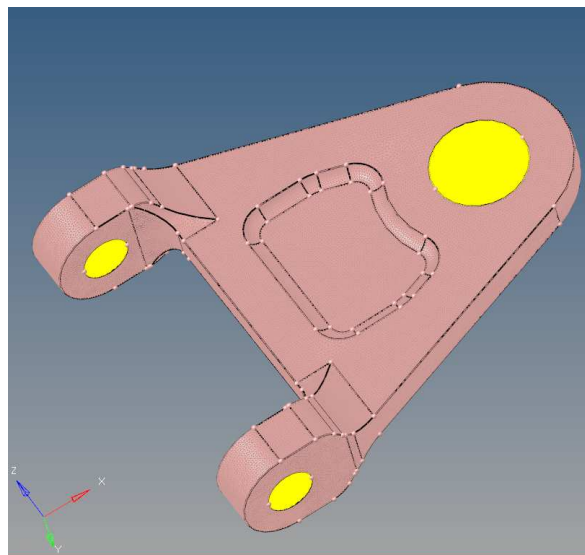


Figure 5.3: FEM model on Altair Hyperworks

### 5.1.2 Material and Property

The main design was created to be manufactured by traditional methods. So cast Ti6Al4V material properties were used for the analysis. Figure 5.4 shows how the material is defined on Hyperworks. Elastic of modulus (E), Poissons's Ratio (Nu) and density (RHO) should be defined on Hypermesh as material properties.


Solver Keyword	MAT1
Name	Titanium_Cast
ID	2
Color	
Include	[Master Model]
Defined	<input checked="" type="checkbox"/>
Card Image	MAT1
User Comments	Hide In Menu/Export
E	114000.0
G	
NU	0.31
RHO	4.429e-009

Figure 5.4: Material view on Altair Hyperworks


Solver Keyword	PSOLID
Name	Design
ID	1
Color	
Include	[Master Model]
Defined	<input checked="" type="checkbox"/>
Card Image	PSOLID
Material	(2) Titanium_Cast

Figure 5.5: Property panel view on Altair Hyperworks

After definition of the material, property should be assigned for each element group. Our mesh was solid and only one material was used, therefore “PSOLID” Card and Cast Ti6Al4V material were used for property definition on Hypermesh. Figure 5.5 shows the property definition panel on Hyperworks.

### 5.1.3 Load Collectors and Load Steps

Loads and boundary conditions were predefined by analysis engineers according to the system work principle and aerodynamic loads. There are five different load cases for the part, and Table 5.1 shows the forces to be applied for each case according to aircraft coordinate system.

The part was constrained by bolt nut connections and degree of freedom for each connection is shown in Figure 5.7. The constraints were located on calculated center nodes of bolt attachment holes, and loads were applied on calculated center node of bushing attachment.

Every force and constraint were defined separately on Hyperworks and with load

Table 5.1: Loads according to analysis coordinate system

	<b>X COMPONENT [N]</b>	<b>Y COMPONENT [N]</b>	<b>Z COMPONENT [N]</b>
<b>FORCE 1</b>	-117.5	0	7476.1
<b>FORCE 2</b>	-731.9	0	-6662.4
<b>FORCE 3</b>	1472.6	0	7060.0
<b>FORCE 4</b>	238.0	0	-6988.2
<b>FORCE 5</b>	-3018.9	0	6349.4

Name	Value
Solver Keyword	SUBCASE
Name	Load Step 1
ID	1
Include	[Master Model]
User Comments	Hide In Menu/Export
<b>Subcase Definition</b>	
Analysis type	Linear Static
SPC	(1) CONSTRAINTS
LOAD	(2) FORCE_1

Figure 5.6: First load step creation on Hyperworks

step panel, load cases were created for each force-constraint combination. Figure 5.6 illustrates the creation of first load case of the analysis. In each load case, same constraints were used, i.e. only forces were changed.

Figure 5.7 represents the force-constraint combination on Hypermesh screen for first load case.

#### 5.1.4 Static Analysis and Results

Optistruct tool was used for analysis of each load case. Hyperview was used to examine and simulate the solutions. Figure 5.8 shows the static analysis result of first load case on Hyperview.

Results for each load case are shown in Table 5.2. Reserve factor(RF) and Maximum UTS for Ti6Al4V are also given in the table.

RF is the ratio of maximum von-Mises stress of the design and material. It should be higher than 1 for a safe design solution. As shown in the table, main design is in the safe region for each case.

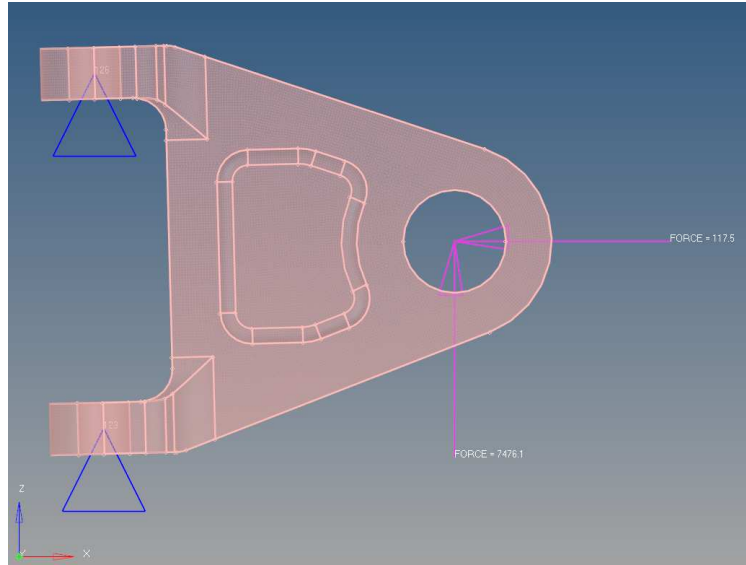


Figure 5.7: Hypermesh view for the first load case

Table 5.2: Static analysis results for the main design

	<b>Max. Von-Mises Stress [MPa]</b>	<b>Max. UTS for Cast Ti6Al4V [MPa]</b>	<b>RF</b>
<b>LOAD CASE 1</b>	716.1	860.0	1.20
<b>LOAD CASE 2</b>	633.6	860.0	1.36
<b>LOAD CASE 3</b>	660.3	860.0	1.30
<b>LOAD CASE 4</b>	670.1	860.0	1.28
<b>LOAD CASE 5</b>	624.2	860.0	1.37

## 5.2 Usage of the Properties Gained from Experiment

As shown in the Table 5.2, there is a chance to optimize the part according to cast material properties and machining restrictions until it reaches to max allowable stress values. In addition to those, AM gives chance to higher allowable stress values and flexibility to manufacture complex parts.

Maximum UTS and YS for X, Y and Z directions were obtained from the experiment. Therefore, a planar approach may be conducted while choosing how to locate part in machine. Planar stress components where maximum von-Mises stresses occur for critical load cases are examined and part is oriented with respected to the plane where maximum stress components occur and the direction of the part is chosen according to the resultant of stress components and oriented to the direction of machine where

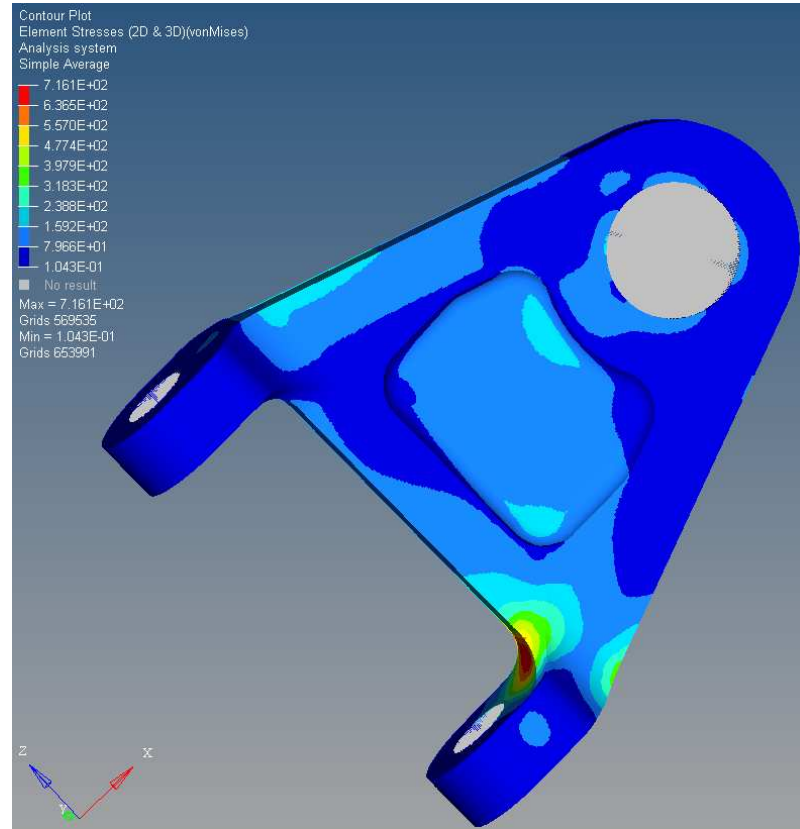


Figure 5.8: Maximum von-mises stresses plot for load case 1 on Hyperview

Table 5.3: Planar stress components at maximum von-mises stress location for critical load case

	<b>X Component [MPa]</b>	<b>Y Component [MPa]</b>	<b>Z Component [MPa]</b>
<b>LOAD CASE 1</b>	236.9	16.8	505.9

maximum UTS values are displayed.

In this study, to obtain lighter component without varying the performance and with the advantage of AM, two topology optimizations were done for the parts to be built in horizontal and vertical directions by using experimental data and with a proper solution for manufacturing.

As seen in Table 5.2, load case 1 is the most critical case where maximum von-Mises stress value is the highest. Planar stress components at the location of maximum von-Mises stress for this case are represented in Table 5.3.

As seen, XZ plane is where the higher stress components exist. Direction of the resul-

tant stress components in this plane is represented in Figure 5.9. For the main design, the angle was found as  $65^\circ$  by using the values of X and Z components in the Table 5.3.

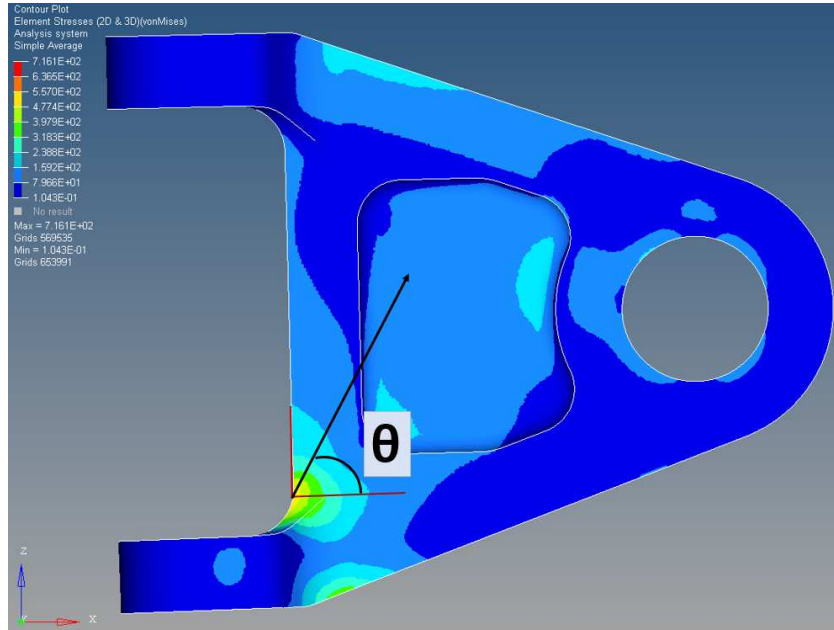


Figure 5.9: Direction of resultant stress component at XZ plane according to analysis coordinate system

Therefore, to locate the main design vertically, XZ plane of the part can be placed to YZ plane of the machine. YZ plane can be chosen instead of XZ plane since Y specimens displayed higher tensile properties in experiment. On the other hand, the direction of the maximum stress may not be placed to the Z direction where highest tensile strength showed in experiment because of the unfeasible solution for manufacturability by considering support geometry creation and unpredictable surface imperfections. Instead, a near solution close to Z direction can be chosen as shown in Figure 5.10.

To orient the main design horizontally in the machine, XZ plane of the part can be placed to XY plane of the machine. And direction of the maximum stress can be located to Y direction of the machine since Y specimens displayed higher strength values than X specimens. Desired location for the horizontal parts are also represented in Figure 5.10

The recommendation for the orientation of the part in the machine was given according to the experimental data in this study. However, to find optimal location for the

parts to be built, scanning pattern should also be considered since differences between X and Y specimens are mainly because of the scanning strategy.

For optimizations, the average value of the Z specimens from the experiment was used for the part to be built vertically. For the horizontal part, the average value of X and Y specimens was used.

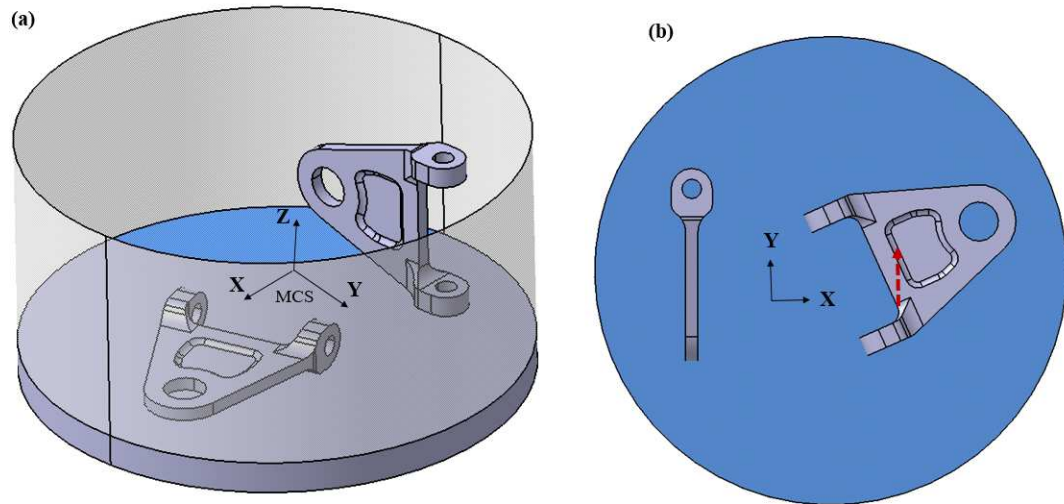


Figure 5.10: Desired locations for the vertical and horizontal parts according to machine/work coordinate system (a) isometric view on machine (b) top view on machine

### 5.3 Optimization Steps

Through following processes, all coordinate systems shown in figures represent the location of the part on its assembly, i.e. aircraft coordinate system, not the machine coordinate system.

#### 5.3.1 Design and Non-Design Spaces

As mentioned before all system conditions and restrictions are predefined and were not changed in this study. Required fasteners and their sizes, minimum radius for lug-clevis connection, thicknesses at fastener connections were remained the same. While creating design and non-design spaces for the optimization, those conditions were used and minimum changes were done for the beginning of the optimization.

Thickness of the fastener connections, for example, was not changed. Fastener connections were chosen as non-design space with needed lug-clevis radius. Areas restricted with other components were remained as design space to be optimized. Pink regions represent the non-design spaces and blue region represents the design space in Figure 5.11.

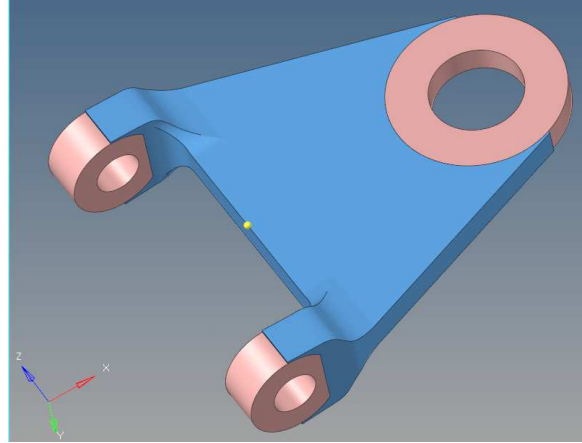


Figure 5.11: Design and non-design spaces

### 5.3.2 Finite Element Model

The same procedure was done for the FEM model as the main design. But for optimization, two different components were defined on Hypermesh for design and non-design regions. And connections between elements were identified on the solver.

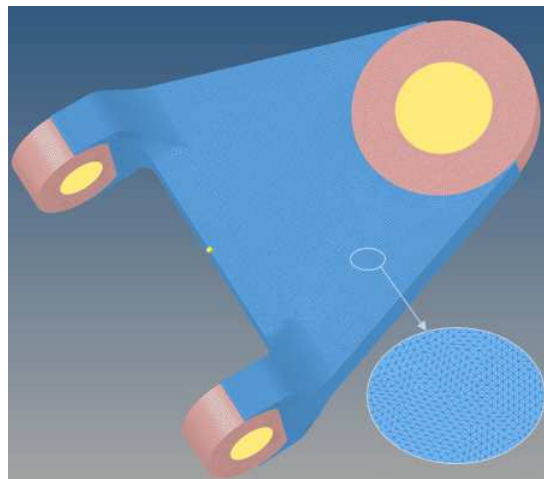


Figure 5.12: FEM model of optimization model on Hypermesh



### 5.3.3 Material and Property

Material definitions were done according to the experimental data. For the first topology optimization, the average of the E values of X and Y specimens was used as 143.68 GPa for horizontal optimization part, and the average value of Z specimens was used as 156.40 GPa for vertical optimization part.

Two different properties with the same material were defined for each optimization model as design and non-design properties. Each property was assigned to the related component.

### 5.3.4 Load collectors and Load Steps

Same values of the main design were used for loads, constraints and load cases as given in Section 5.1.3.

### 5.3.5 Optimization parameters

To create optimization variables, “Optimization” panel is chosen under analysis tab and new menu for optimization are displayed as Figure 5.13. Used sub-menus are marked by red rectangles on the figure.

topology	size(parameter)	responses
topography	gauge	dconstraints
free size	desvar link	obj reference
free shape		objective
	shape	
composite shuffle	perturbations	
composite size	HyperMorph	

Figure 5.13: Optimization panel on Optistruct

Design variable was created by topology menu and following design constraints were defined for design region.

#### Minimum Member Size

With member size control, it is possible to adjust desirable maximum and minimum member size. In our problem, minimum member size was used to achieve EBM manufacturing constraints. Generally, at least 1mm for the member size is recommended

but because of the roughness of the surfaces on EBM parts, 1.5mm was chosen as the minimum member size to gain feasible last product. It is recommended by the minimum member size to be at least three times larger than the finite element size. That is why 0.5 was used as an element size during meshing.

### Stress Constraint

As mentioned in Optistruct topology optimization example with stress constraints [50], it is possible to see local high stresses after optimization and generally local shape and size optimization are needed after topology optimization. In our problem, it is desired to use final shape only after topology optimization. For this purpose, lower stress constraints were used for optimization of the parts than the test results. After a few iterations, 850MPa and 900MPa were used for horizontal part and for vertical part, respectively.

Both minimum member size and stress constraint were defined under “topology” menu where the design variable was created. Figure 5.13 illustrates the parameters sub-menu to define those constraints.



Figure 5.14: Design variable parameters screen for minimum member size control and stress constraint

### Symmetry

Generally, topology optimization does not give symmetric solutions although design space and constraints are symmetric. On the other hand, a symmetric design is often desirable to manufacture. By using pattern grouping sub-menu under topology tab, it is possible to create symmetric design solutions by Optistruct.

In our problem, one-plane symmetry was used for esthetic of the final design. Plane was created in the middle of the part parallel to XZ plane of aircraft coordinate system. Figure 5.15 illustrates the related pattern grouping sub menu and Figure 5.16 shows how to define symmetry plane.

### Responses, Objective and Constraint

For objective and constraint functions firstly responses should be defined. In our

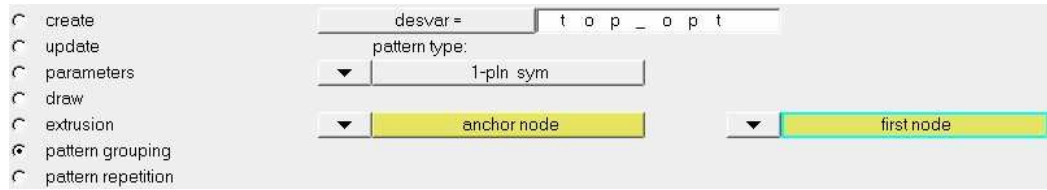


Figure 5.15: Design variable pattern grouping screen for symmetry definition

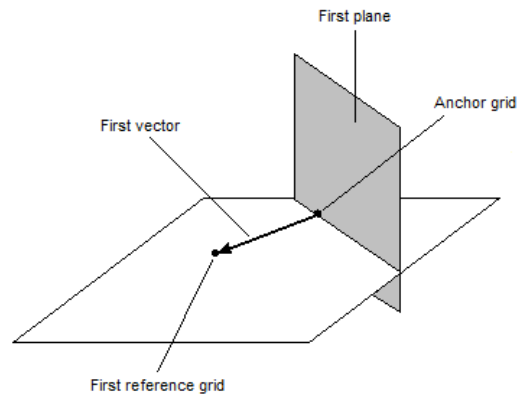


Figure 5.16: Creation of the virtual plane for one plane symmetry as pattern type [51]

optimization problem, it is desired to minimize mass with constrained stress value. Since stress constraint was already defined under design variable sub menu, no response was needed to be created for constraint function. For objective function mass response was created and objective was adjusted to minimize volume on Optistruct.

### 5.3.6 Optimization Results

By using Optistruct, optimization was conducted for each optimization model. Results were examined and simulated via Hyperview tool. Figure 5.17 and Figure 5.19 show the density values between 0 and 1 for horizontal and vertical optimization model, respectively. As seen in the figures, there are minor differences on contour plots. Figure 5.18 and Figure 5.20 show the expected models after optimization with given iso values.

The results were gain after 35 iterations of horizontal model and 32 iterations for vertical model.

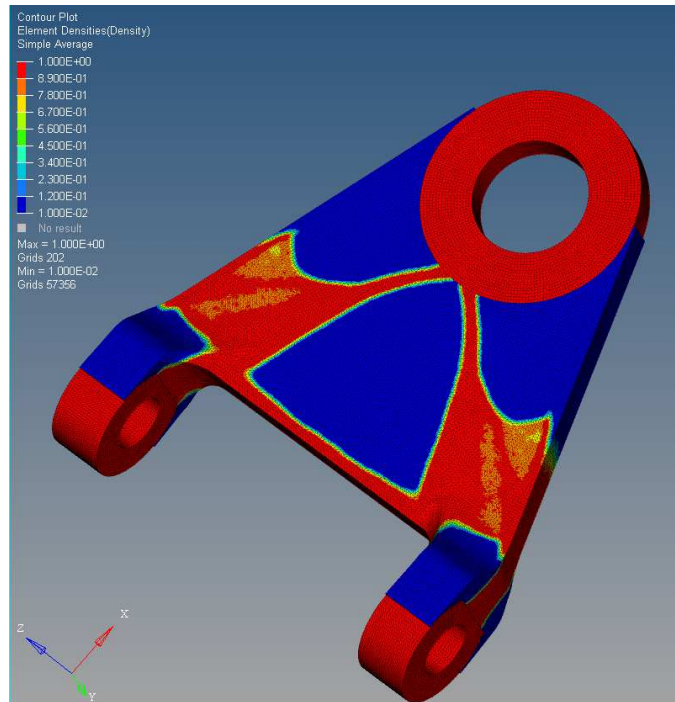


Figure 5.17: Contour plot for optimization results for the part oriented horizontally

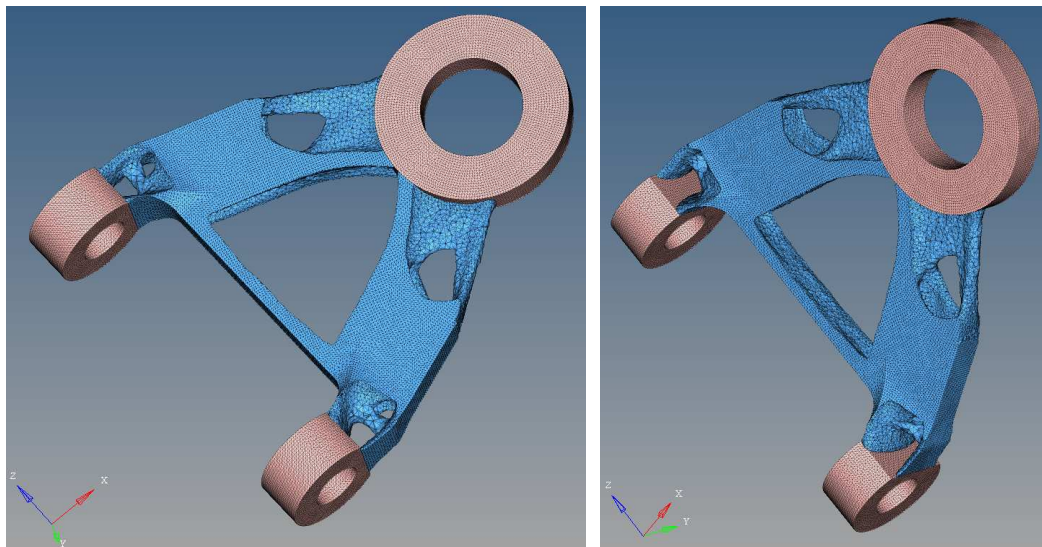


Figure 5.18: Optimization model of the horizontal part for 0.3 iso density value

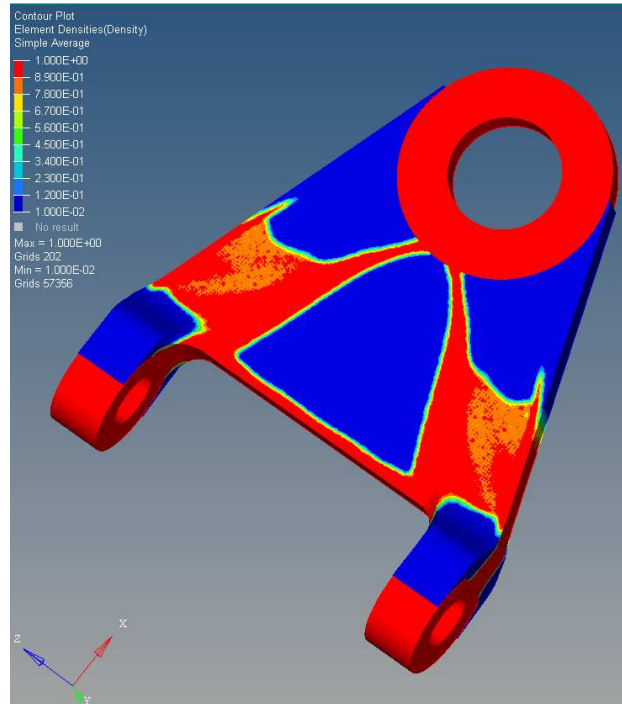


Figure 5.19: Contour plot of optimization results for the part oriented vertically

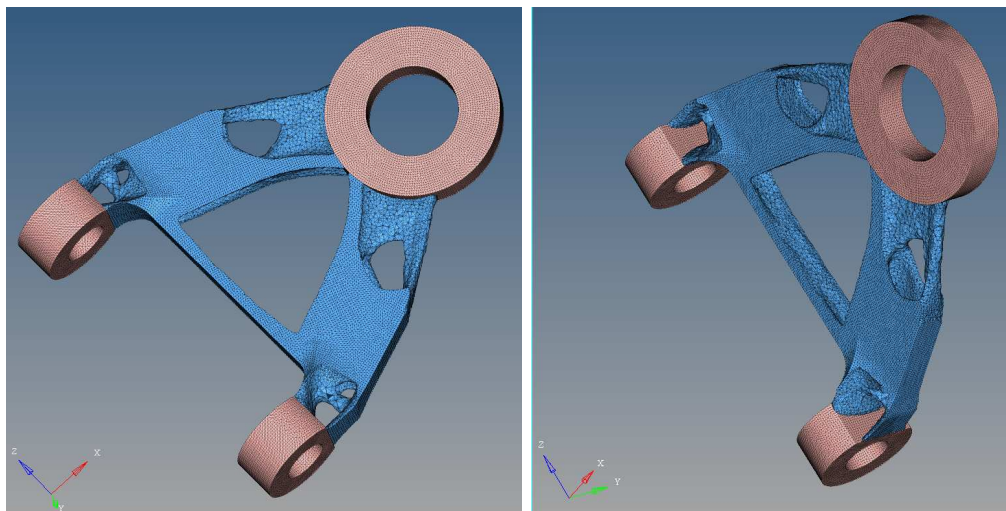


Figure 5.20: Optimization model of the vertical part for 0.35 iso density value

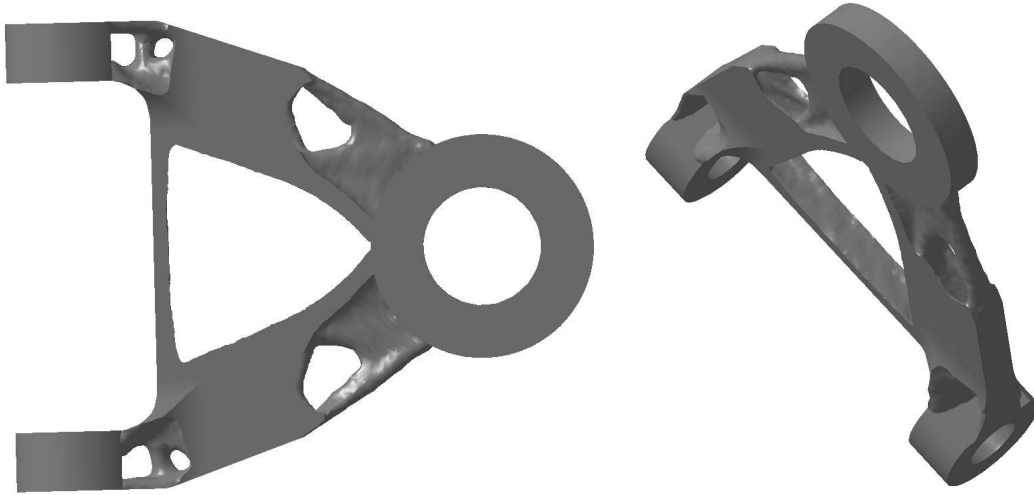


Figure 5.21: Last optimized model for the horizontal part with smooth surfaces

### 5.3.7 CAD Models after Optimization

After iterations on iso values of the results and reanalysis for chosen values of optimization, final models were created via Ossmooth tool on Hyperworks. With this tool, it is possible to create final design by transforming mesh data to surfaces. Ossmooth tool provides smooth surfaces by Laplacian method.

Since those parts were optimized to be manufactured by AM, no need to reshape the geometry is desired and is achieved thanks to this tool.

Figure 5.21, and Figure 5.22 represent the final CAD data of horizontal and vertical optimized parts, respectively. Geometries are too close to each other in visuals. But according to CAD data, horizontal part has 38.8% lower weight and the vertical part has 40.7% lower weight than the main design.

### 5.3.8 Stress Analysis for the Final Models

Optistruct has also capability to reanalysis of the optimization according to given iso values. But to manufacture geometries from optimization results directly, Ossmooth tool was used for smooth surfaces and this affected the final shape and analysis results.

Via Ossmooth tool, remesh operation was conducted for each optimized model by



Figure 5.22: Last optimized model for vertical part with smooth surfaces

remaining constraints and load cases as the same. Analysis was done by Optistruct again and simulated via Hyperview. Figures 5.23 represent the FEM model of optimization models on Hypermesh and Figure 5.24 and Figure 5.25 represent the results of the analysis.

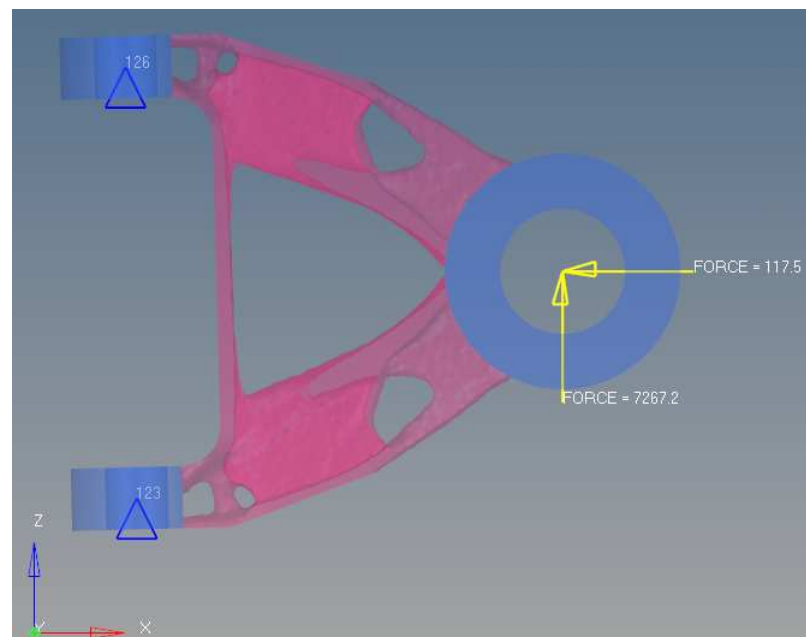


Figure 5.23: Hypermesh view for first load case

Table 5.4 and Table 5.5 show the final results for each optimization model. As shown in the tables, since RFs are close to the value of 1, but still higher, optimization models are in safe region.

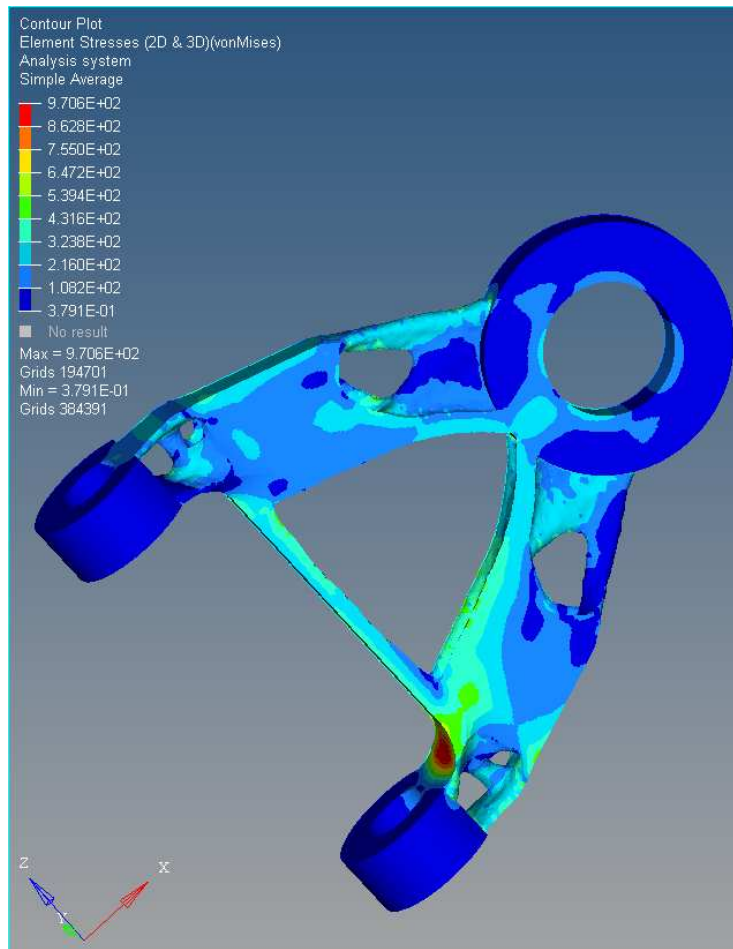


Figure 5.24: Results of the first load case for horizontal part

Table 5.4: Static analysis results for the parts to be built horizontally

	Max. Von-Mises Stress [MPa]	Max. UTS for Horizontal EBM Ti6Al4V [MPa]	RF
<b>LOAD CASE 1</b>	970.6	979.9	1.01
<b>LOAD CASE 2</b>	887.8	979.9	1.10
<b>LOAD CASE 3</b>	939.0	979.9	1.04
<b>LOAD CASE 4</b>	933.7	979.9	1.05
<b>LOAD CASE 5</b>	855.3	979.9	1.15



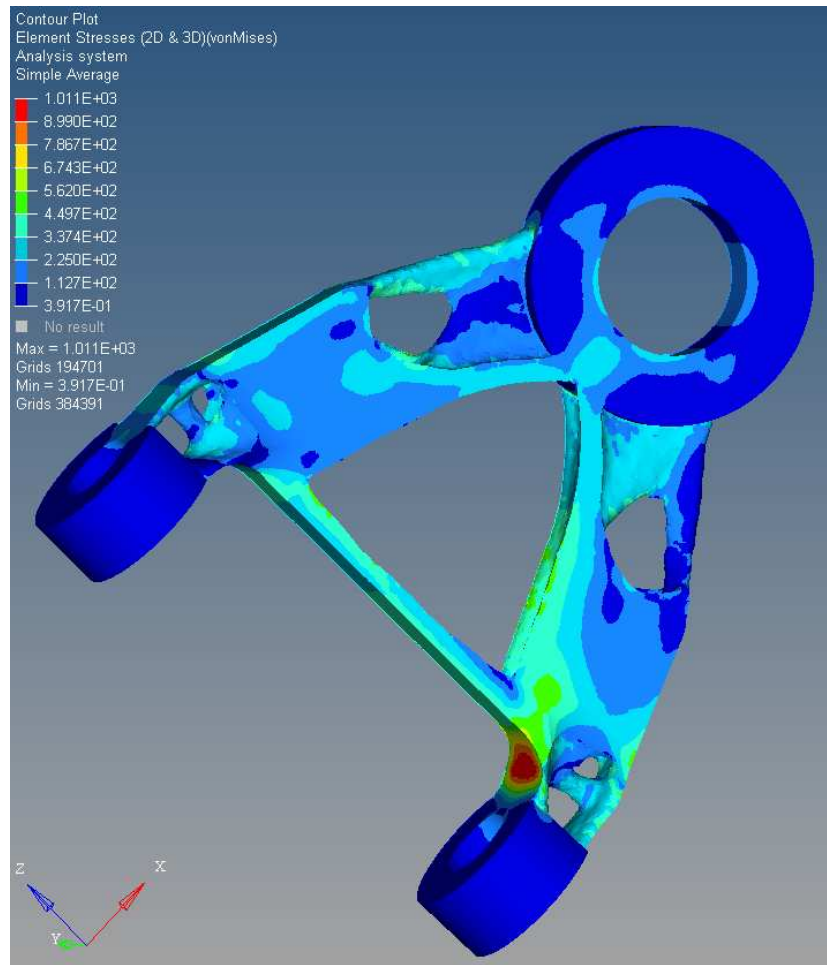


Figure 5.25: Results of the first load case for vertical part

Table 5.5: Static analysis results for the parts to be built vertically

	Max. Von-Mises Stress [MPa]	Max. UTS for Vertical EBM Ti6Al4V [MPa]	RF
<b>LOAD CASE 1</b>	1011.0	1023.8	1.01
<b>LOAD CASE 2</b>	898.9	1023.8	1.14
<b>LOAD CASE 3</b>	950.5	1023.8	1.08
<b>LOAD CASE 4</b>	945.7	1023.8	1.08
<b>LOAD CASE 5</b>	867.4	1023.8	1.18

## 5.4 Comparison of the Main Design and Optimized Models

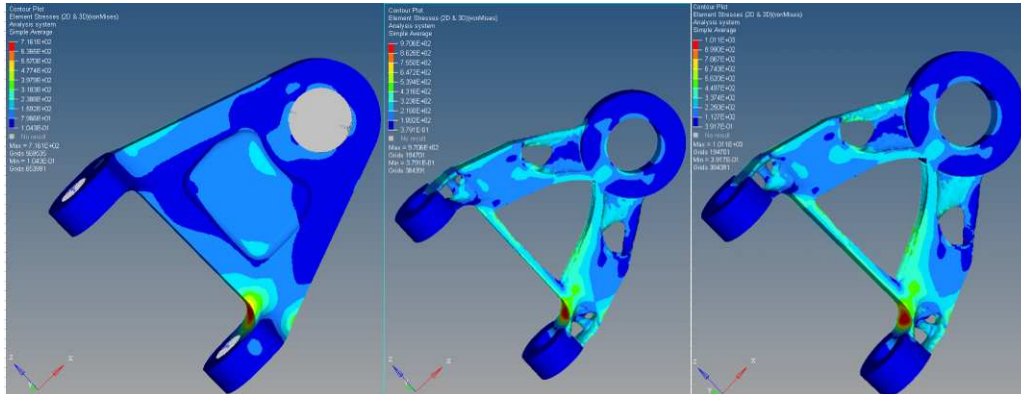


Figure 5.26: Comparison of (a)The main design, (b)Optimized horizontal part, (c) Optimized vertical part

As mentioned before, according to CAD data, horizontal part has 38.8% and the vertical part has 40.7% lower weight than the main design. In addition to higher mechanical properties of EBM, differences between the analysis results of the main design and optimized parts are also because of the fact that main design is in the over safe region. By decreasing the RF values, lighter parts were obtained.

Difference between the horizontal and vertical optimized parts, on the other hand, is because of the difference allowable stresses but they are still similar in shape due to load distribution on part.

The vertical optimization part was produced by ARCAM Q20 EBM using Ti6Al4V. The part was manufactured with the same process parameters used in the experimental part. The pictures of the final product can be seen in Figure 5.27. The weight of



Figure 5.27: As-built vertical optimization part

the product was matching the CAD data and surface imperfections were observed as expected. Machining and other surface finishing methods can be investigated to improve aesthetics and also the fatigue life which is beyond the scope of this study. While it is possible to manufacture main model by EBM method, it is not possible to manufacture optimized models by a traditional machine center since they have cavities that cannot be reached by cutting tools. Even if the optimized models could be produced by traditional method, they would fail due to lower tensile properties of the cast material.



## CHAPTER 6

### CONCLUSION AND FUTURE WORK

The presented study focused on the investigation of the effects of building direction on mechanical properties of Ti6Al4V parts produced by EBM and topology optimization of an aircraft fitting according to mechanical properties obtained from the experiments.

The following conclusions can be drawn from the study:

- Z specimens (i.e., vertical parts) that were built parallel to applied force, have better results on UTS, YS and E than X and Y specimens (i.e., horizontal parts) that were built perpendicular to applied load. Z specimens have also lower elongation rates at fracture than X and Y specimens.
- EBM parts have better tensile properties compared to cast and wrought material.
- Due to nature of the process, as-built parts have higher surface roughness values compared to cast and wrought material.
- Higher surface roughness of EBM parts results with lower elongation rates.
- Machining of the rough surfaces does not affect the tensile properties directly. But elongation rates increase with improving surface finish.
- EBM parts display a mixed ductile-brittle behavior, but ductility is dominating.
- Topology optimization is an effective method to create complex and lighter shapes without varying the function of the components. AM gives chance to manufacture of those complex parts directly.

- It is possible to have lighter parts by using capability of EBM technology and better mechanical properties of powder material.

AM is a rising technology and Electron Beam Melting has a good potential for manufacturing end-use metallic parts. There are lots of research topics on this technology and the number of them is increasing day by day. The following topics may be considered as future work of this study:

- The effect of building direction on fatigue properties of Ti6Al4V parts produced by EBM.
- The effect of residual stress on fatigue properties of Ti6Al4V parts produced by EBM.
- The effects of heat treatment and surface finish operations on fatigue life of Ti6Al4V parts produced by EBM.
- Combined topology, shape and sizing optimization for AM.
- Optimization of the lattice structures produced by EBM.
- Manufacturing and testing optimization model of EBM parts and comparing results with theoretical data.

## REFERENCES

- [1] Kruth, J. (1991). Material Increase Manufacturing by Rapid Prototyping Techniques. *CIRP Annals*, 40(2), 603-614. doi:10.1016/s0007-8506(07)61136-6
- [2] Levy, G. N., Schindel, R., & Kruth, J. (2003). Rapid Manufacturing And Rapid Tooling With Layer Manufacturing (Lm) Technologies, State Of The Art And Future Perspectives. *CIRP Annals*, 52(2), 589-609. doi:10.1016/s0007-8506(07)60206-6
- [3] Hrabe, N., & Quinn, T. (2013). Effects of processing on microstructure and mechanical properties of a titanium alloy (Ti-6Al-4V) fabricated using electron beam melting (EBM), part 1: Distance from build plate and part size. *Materials Science and Engineering: A*, 573, 264-270. doi:10.1016/j.msea.2013.02.064
- [4] Edwards, P., Oconner, A., & Ramulu, M. (2013). Electron Beam Additive Manufacturing of Titanium Components: Properties and Performance. *Journal of Manufacturing Science and Engineering*, 135(6), 061016. doi:10.1115/1.4025773
- [5] Brackett D., Ashcroft I., & Hague R. (2011). Topology Optimization for Additive Manufacturing. SFF Symposium, Austin, TX.
- [6] Welsch, G., Boyer, R., & Collings, E. W. (1994). Materials properties handbook: Titanium alloys. Materials Park, OH: ASM International
- [7] Murr, L., Esquivel, E., Quinones, S., Gaytan, S., Lopez, M., Martinez, E., . . . Wicker, R. (2009). Microstructures and mechanical properties of electron beam-rapid manufactured Ti-6Al-4V biomedical prototypes compared to wrought Ti-6Al-4V. *Materials Characterization*, 60(2), 96-105. doi:10.1016/j.matchar.2008.07.006
- [8] Koike, M., Greer, P., Owen, K., Lilly, G., Murr, L. E., Gaytan, S. M., . . . Okabe, T. (2011). Evaluation of Titanium Alloys Fabricated Using Rapid Prototyp-

- ing Technologies—Electron Beam Melting and Laser Beam Melting. *Materials*, 4(10), 1776-1792. doi:10.3390/ma4101776
- [9] Zhai, Y., Galarraga, H., & Lados, D. A. (2015). Microstructure Evolution, Tensile Properties, and Fatigue Damage Mechanisms in Ti-6Al-4V Alloys Fabricated by Two Additive Manufacturing Techniques. *Procedia Engineering*, 114, 658-666. doi:10.1016/j.proeng.2015.08.007
- [10] Formanoir, C. D., Michotte, S., Rigo, O., Germain, L., & Godet, S. (2016). Electron beam melted Ti-6Al-4V: Microstructure, texture and mechanical behavior of the as-built and heat-treated material. *Materials Science and Engineering: A*, 652, 105-119. doi:10.1016/j.msea.2015.11.052
- [11] Wauthle, R., Vrancken, B., Beynaerts, B., Jorissen, K., Schrooten, J., Kruth, J., & Humbeeck, J. V. (2015). Effects of build orientation and heat treatment on the microstructure and mechanical properties of selective laser melted Ti6Al4V lattice structures. *Additive Manufacturing*, 5, 77-84. doi:10.1016/j.addma.2014.12.008
- [12] Wycisk, E., Emmelmann, C., Siddique, S., & Walther, F. (2013). High Cycle Fatigue (HCF) Performance of Ti-6Al-4V Alloy Processed by Selective Laser Melting. *Advanced Materials Research*, 816-817, 134-139. doi:10.4028/www.scientific.net/amr.816-817.134
- [13] Gong, H., Rafi, K., Gu, H., Ram, G. J., Starr, T., & Stucker, B. (2015). Influence of defects on mechanical properties of Ti-6Al-4V components produced by selective laser melting and electron beam melting. *Materials & Design*, 86, 545-554. doi:10.1016/j.matdes.2015.07.147
- [14] Al-Bermani, S. S., Blackmore, M. L., Zhang, W., & Todd, I. (2010). The Origin of Microstructural Diversity, Texture, and Mechanical Properties in Electron Beam Melted Ti-6Al-4V. *Metallurgical and Materials Transactions A*, 41(13), 3422-3434. doi:10.1007/s11661-010-0397-x
- [15] Carroll, B. E., Palmer, T. A., & Beese, A. M. (2015). Anisotropic tensile behavior of Ti-6Al-4V components fabricated with directed en-



- ergy deposition additive manufacturing. *Acta Materialia*, 87, 309-320. doi:10.1016/j.actamat.2014.12.054
- [16] Wang, X., Gong, X., & Chou, K. (2015). Scanning Speed Effect on Mechanical Properties of Ti-6Al-4V Alloy Processed by Electron Beam Additive Manufacturing. *Procedia Manufacturing*, 1, 287-295. doi:10.1016/j.promfg.2015.09.026
- [17] Algardh, J. K., Horn, T., West, H., Aman, R., Snis, A., Engqvist, H., . . . Harrysson, O. (2016). Thickness dependency of mechanical properties for thin-walled titanium parts manufactured by Electron Beam Melting (EBM) ®. *Additive Manufacturing*, 12, 45-50. doi:10.1016/j.addma.2016.06.009
- [18] Tang, H. P., Qian, M., Liu, N., Zhang, X. Z., Yang, G. Y., & Wang, J. (2015). Effect of Powder Reuse Times on Additive Manufacturing of Ti-6Al-4V by Selective Electron Beam Melting. *Jom*, 67(3), 555-563. doi:10.1007/s11837-015-1300-4
- [19] Edwards, P., Oconner, A., & Ramulu, M. (2013). Electron Beam Additive Manufacturing of Titanium Components: Properties and Performance. *Journal of Manufacturing Science and Engineering*, 135(6), 061016. doi:10.1115/1.4025773
- [20] Antonysamy, A., Meyer, J., & Prangnell, P. (2013). Effect of build geometry on the  $\beta$ -grain structure and texture in additive manufacture of Ti6Al4V by selective electron beam melting. *Materials Characterization*, 84, 153-168. doi:10.1016/j.matchar.2013.07.012
- [21] Viqaruddin, M., & Reddy, D. R. (2017). Structural optimization of control arm for weight reduction and improved performance. *Materials Today: Proceedings*, 4(8), 9230-9236. doi:10.1016/j.matpr.2017.07.282
- [22] Vasudeva, R., & Soundararajan S. (2012). Optimization of Front Axle Mounts Vibration Characteristics for Driveline Integration with Chassis. General Motors Technical Center, India. Retrieved from: <https://www.altairatc.com/>
- [23] Sreedhar, B., & Sasidhar, N.(2012). Optimization of Mounting Bracket. Hyundai Motor, India. Retrieved from: <https://www.altairatc.com/>

- [24] Walton, D., & Moztarzadeh, H. (2017). Design and Development of an Additive Manufactured Component by Topology Optimisation. *Procedia CIRP*, 60, 205-210. doi:10.1016/j.procir.2017.03.027
- [25] Marchesi, T. R., Lahuerta, R. D., Silva, E. C., Tsuzuki, M. S., Martins, T. C., Barari, A., & Wood, I. (2015). Topologically Optimized Diesel Engine Support Manufactured with Additive Manufacturing. *IFAC-PapersOnLine*, 48(3), 2333-2338. doi:10.1016/j.ifacol.2015.06.436
- [26] CADimensions, Inc. | Expert SOLIDWORKS Sales, Training and Support. (n.d.). Retrieved from <http://www.cadimensions.com/>
- [27] Deutsch - Fraunhofer IWU. (n.d.). Retrieved from <http://www.iwu.fraunhofer.de/>
- [28] Nano News Net. (n.d.). Retrieved from <http://www.nanonewsnet.ru/>
- [29] Lasers Today. (n.d.). Retrieved from <https://www.laserstoday.com/>
- [30] Williams, S. W., Martina, F., Addison, A. C., Ding, J., Pardal, G., & Colegrove, P. (2015). Wire Arc Additive Manufacturing. *Materials Science and Technology*, 32(7), 641-647.
- [31] Guo, J., Zhou, Y., Liu, C., Wu, Q., Chen, X., & Lu, J. (2016). Wire Arc Additive Manufacturing of AZ31 Magnesium Alloy: Grain Refinement by Adjusting Pulse Frequency. *Materials*, 9(10), 823. doi:10.3390/ma9100823
- [32] Arcam Q20plus. (n.d.). Retrieved from <http://www.arcam.com/technology/products/arcam-q20/>
- [33] Weiwei, H., Wenpeng, J., Haiyan, L., Huiping, T., Xinting, K., & Yu, H. (2011). Research on Preheating of Titanium Alloy Powder in Electron Beam Melting Technology. *Rare Metal Materials and Engineering*, 40(12), 2072-2075.
- [34] Bendsoe, M. P., & Sigmund, O. (2003). Topology optimization: *Theory, methods, and applications*. Berlin: Springer.
- [35] Leiva, J. P.(2004). Topometry Optimization: A New Capability to Perform Element by Element Sizing Optimization of Structures. 10th AIAA/ISSMO Symposium on Multidisciplinary Analysis and Optimization, Albany, NY.

- [36] Leiva, J. P.(2003). Methods for Generation Perturbation Vectors for Topography Optimization of Structures. 5th World Congress of Structural and Multidisciplinary Analysis and Optimization, Lido di Jesolo, Italy.
- [37] Additive Manufacturing for Implants and Aerospace, EBM. (n.d.). Retrieved from <http://www.arcam.com/>
- [38] Klassen, A., Forster, V. E., Juechter, V., & Körner, C. (2017). Numerical simulation of multi-component evaporation during selective electron beam melting of TiAl. *Journal of Materials Processing Technology*, 247, 280-288. doi:10.1016/j.jmatprotec.2017.04.016
- [39] Tammias-Williams, S., Zhao, H., Léonard, F., Derguti, F., Todd, I., & Prangnell, P. (2015). XCT analysis of the influence of melt strategies on defect population in Ti-6Al-4V components manufactured by Selective Electron Beam Melting. *Materials Characterization*, 102, 47-61. doi:10.1016/j.matchar.2015.02.008
- [40] Lu, W., Lin, F., Han, J., Qi, H., & Yan, N. (2009). Scan strategy in electron beam selective melting. *Tsinghua Science and Technology*, 14(S1), 120-126. doi:10.1016/s1007-0214(09)70078-1
- [41] Everhart, W., Dinardo, J., & Barr, C. (2016). The Effect of Scan Length on the Structure and Mechanical Properties of Electron Beam-Melted Ti-6Al-4V. *Metallurgical and Materials Transactions A*, 48(2), 697-705. doi:10.1007/s11661-016-3866-z
- [42] Suard, M. (2006). *Characterization and optimization of lattice structures made by Electron Beam Melting*, Phd Thesis, Universite de Grenoble, France.
- [43] Schulze, C., Weinmann, M., Schweigel, C., Keßler, O., & Bader, R. (2018). Mechanical Properties of a Newly Additive Manufactured Implant Material Based on Ti-42Nb. *Materials*, 11(1), 124. doi:10.3390/ma11010124
- [44] Shunmugavel, M., Polishetty, A., & Littlefair, G. (2015). Microstructure and Mechanical Properties of Wrought and Additive Manufactured Ti-6Al-4V Cylindrical Bars. *Procedia Technology*, 20, 231-236. doi:10.1016/j.protcy.2015.07.037

- [45] Quénard, O., Dorival, O., Guy, P., Votié, A., & Brethome, K. (2018). Measurement of Fracture Toughness of Metallic Materials Produced by Additive Manufacturing. *CEAS Space Journal*, 10(3), 343-353.
- [46] Galarraga, H., Lados, D. A., Dehoff, R. R., Kirka, M. M., & Nandwana, P. (2016). Effects of the microstructure and porosity on properties of Ti-6Al-4V ELI alloy fabricated by electron beam melting (EBM). *Additive Manufacturing*, 10, 47-57. doi:10.1016/j.addma.2016.02.003
- [47] Mills, K. (1985). *ASM Handbook. Volume 9. Metallography and microstructures*. Materials Park, OH: ASM International.
- [48] Rafi, H. K., Karthik, N. V., Gong, H., Starr, T. L., & Stucker, B. E. (2013). Microstructures and Mechanical Properties of Ti6Al4V Parts Fabricated by Selective Laser Melting and Electron Beam Melting. *Journal of Materials Engineering and Performance*, 22(12), 3872-3883. doi:10.1007/s11665-013-0658-0
- [49] B.S. Bass(2008). *Validating the Arcam EBM process as an alternative fabrication method for titanium-6Al-4V alloys*, Ms Thesis, N. C. State Univ., USA.
- [50] Topology Optimization of a Hook with Stress Constraint (n.d.). Retrieved from [https://connect.altair.com/CP/SA/training/self\\_paced/optimization/content/opt3/pdf/ex1b.pdf](https://connect.altair.com/CP/SA/training/self_paced/optimization/content/opt3/pdf/ex1b.pdf)
- [51] How to Obtain Symmetric Concepts with Topology Optimization. (n.d.). Retrieved from [https://altairuniversity.com/wp-content/uploads/2015/11/tutorial\\_topology-optimization-with-pattern-grouping.pdf](https://altairuniversity.com/wp-content/uploads/2015/11/tutorial_topology-optimization-with-pattern-grouping.pdf)